© 2018. Published by The Company of Biologists Ltd | Development (2018) 145, dev155283. doi:10.1242/dev.155283

RESEARCH ARTICLE

RBX2 maintains final retinal cell position in a DAB1-dependent and -independent fashion

Corinne L. Fairchild[1], Keiko Hino[1], Jisoo S. Han[1], Adam M. Miltner[1], Gabriel Peinado Allina[1], Caileigh E. Brown[1], Marie E. Burns[1,2], Anna La Torre[1,*] and Sergi Simó[1,*,‡]

ABSTRACT

The laminated structure of the retina is fundamental for the organization of the synaptic circuitry that translates light input into patterns of action potentials. However, the molecular mechanisms underlying cell migration and layering of the retina are poorly understood. Here, we show that RBX2, a core component of the E3 ubiquitin ligase CRL5, is essential for retinal layering and function. RBX2 regulates the final cell position of rod bipolar cells, cone photoreceptors and Muller glia. Our data indicate that sustained RELN/DAB1 signaling, triggered by depletion of RBX2 or SOCS7 – a CRL5 substrate adaptor known to recruit DAB1 – causes rod bipolar cell misposition. Moreover, whereas SOCS7 also controls Muller glia cell lamination, it is not responsible for cone photoreceptor positioning, suggesting that RBX2, most likely through CRL5 activity, controls other signaling pathways required for proper cone localization. Furthermore, RBX2 depletion reduces the number of ribbon synapses and disrupts cone photoreceptor function. Together, these results uncover RBX2 as a crucial molecular regulator of retina morphogenesis and cone photoreceptor function.

KEY WORDS: Retina development, Neuron migration, CRL5, RBX2, DAB1

INTRODUCTION

The mammalian retina, similar to other regions of the central nervous system (CNS), develops from a pseudostratified neuroepithelium into a laminated tissue in which neuronal subtypes are arranged in distinctive layers: the outer nuclear layer (ONL) comprises cone and rod photoreceptors; the inner nuclear layer (INL) contains bipolar, horizontal and amacrine cells as well as Muller glia cell bodies; and the ganglion cell layer (GCL) contains the somas of the retinal ganglion cells and displaced amacrine cells. The processes of these different neurons are stacked in alternating layers; hence the cell bodies are located in the ONL, INL and GCL, and the processes and synaptic contacts in the outer plexiform layer (OPL) and inner plexiform layer (IPL) (Kolb et al., 1992; Rodieck, 1973).

During retinal development, all progenitor cells exit the cell cycle at the most apical part of the retina and, therefore, newborn post-mitotic cells need to migrate different distances until they reach their final layer (Baye and Link, 2008; Chow et al., 2015; Edqvist and Hallbook, 2004; Morgan et al., 2006). Several modes of migration have been described, including somal translocation, multipolar and bipolar migration (Chow et al., 2015; Edqvist and Hallbook, 2004; Icha et al., 2016; Krol et al., 2016); however, the molecular mechanisms that regulate the mode of migration, persistence or migration termination remain for the most part elusive.

The extracellular glycoprotein reelin (RELN) is essential during neuron migration in the CNS (Rice and Curran, 2001; Tissir and Goffinet, 2003), and *Reln* mutant mice (*reeler*) exhibit severe patterning defects (Goffinet, 1983; Lambert de Rouvroit and Goffinet, 1998; Miyata et al., 1997; Tissir and Goffinet, 2003). However, although RELN and its downstream effectors are also expressed in the retina (Rice and Curran, 2000; Trotter et al., 2011), no gross migration defects have been reported in the retinas of reeler mice (Rice and Curran, 2001).

Binding of RELN to its receptors, APOER2 and VLDLR, promotes the phosphorylation of the adaptor protein DAB1 by the tyrosine kinases FYN and SRC, transducing the RELN signal to the soma (Arnaud et al., 2003b; Trommsdorff et al., 1999). Importantly, DAB1 tyrosine phosphorylation (pY-DAB1) also triggers its own degradation in a proteasome-dependent manner, terminating RELN/DAB1 signaling (Arnaud et al., 2003a).

The cullin 5 (CUL5)-RING E3 ubiquitin ligase (CRL5) is the multiprotein complex responsible for polyubiquitylating and targeting pY-DAB1 for degradation (Feng et al., 2007; Simó and Cooper, 2013; Simo et al., 2010). CRL5 nucleates on the CUL5 backbone (Fig. 1A). On its C terminus, CUL5 binds the RING protein RBX2 (also known as RNF7), which recruits Ub~E2 enzyme (Petroski and Deshaies, 2005). On its N terminus, CUL5 binds to the elongin B/C (ELOB and ELOC) proteins to promote association with substrate adaptor proteins responsible for binding and recruiting targeted substrates (Okumura et al., 2016). To date, at least 38 different substrate adaptors have been identified for CRL5, including eight SOCS proteins (SOCS1-SOCS7 and CISH) that can bind to tyrosine-phosphorylated substrates through an SH2 domain (Okumura et al., 2016). It has been previously shown that SOCS6 and SOCS7 bind and target DAB1 for degradation in the neocortex (Lawrenson et al., 2017; Simo and Cooper, 2013). Importantly, depletion of RBX2, which renders CRL5 inactive, results in the accumulation of pY-DAB1 and subsequent dispersion of cortical projection neurons. Similarly, normal cerebellar development also requires RBX2. However, proper cerebellar layering does not require SOCS7, highlighting the importance of different SOCS adaptors (Simó and Cooper, 2013).

Here, we provide evidence that all the different components of CRL5 are expressed in the murine eye and that loss of RBX2 results in microphthalmia, ptosis and cataracts. We further demonstrate that RBX2 regulates the final position of rod bipolar cells (rBCs), cone

[1]Department of Cell Biology and Human Anatomy, University of California Davis, CA 95616, USA. [2]Department of Ophthalmology and Vision Science, University of California Davis, CA 95616, USA.
*Co-senior authors

‡Author for correspondence (ssimo@ucdavis.edu)

S.S., 0000-0002-8344-0313

Received 23 May 2017; Accepted 28 December 2017

Development (2018) 145, dev155283. doi:10.1242/dev.155283

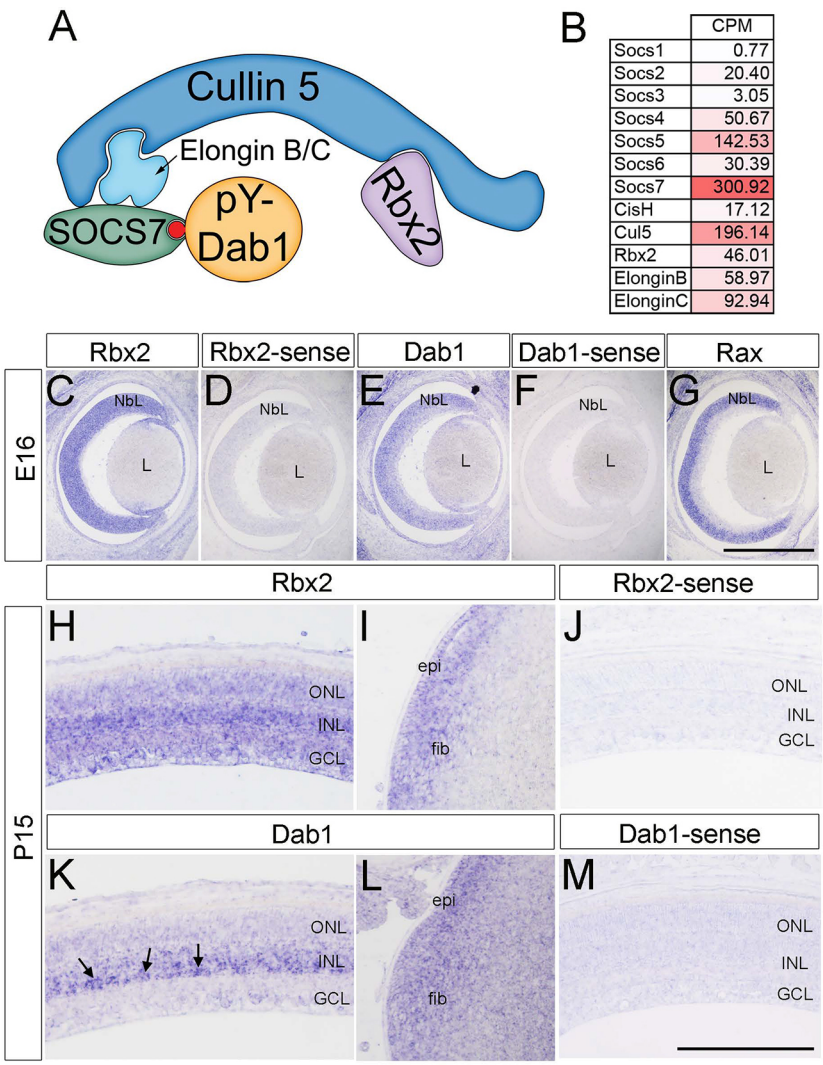

Fig. 1. Several proteins of the CRL5 complex are expressed in the developing retina. (A) CRL5 diagram. SOCS7 is an example of CRL5 substrate adaptor protein bound to tyrosine-phosphorylated DAB1 (pY-DAB1), one of its bona fide substrates. (B) Heat map showing RNA-seq analysis of CRL5 genes in P15 retinas. Data have been normalized and are expressed as counts per million reads (CPM). (C-M) Expression pattern of *Rbx2* and *Dab1* mRNA analyzed by *in situ* hybridization. Paraffin sections of E16 wild-type retinas were hybridized with *Rbx2* (C) and *Dab1* (E) antisense probes. *Rax* antisense probe (G) was used as positive control. Paraffin sections of P15 wild-type mouse retinas were hybridized with *Rbx2* (H,I) and *Dab1* (K,L) antisense probes. *Rbx2* is ubiquitously expressed in the retina, whereas *Dab1* expression was highest in the innermost part of the INL (arrows). Sense probes were used as controls (D,F,J,M). NbL, neuroblastic layer; L, lens; ONL, outer nuclear layer; INL, inner nuclear layer; GCL, ganglion cell layer; epi, epithelium of the lens; fib, lens fibers. Scale bars: 200 µm.

photoreceptors and Muller glia cells (MGCs). In absence of RBX2, rBCs change their position after reaching their intended location at the top of the INL at late stages of development. We also demonstrate that RBX2 depletion causes accumulation of pY-DAB1 in AII-amacrine cells and that reduction of DAB1 levels in RBX2 mutant retinas rescues rBC position. Finally, we show that RBX2 regulates cone ribbon synapses and cone function. Our results support a key role for RBX2, most likely through CRL5 activity, in retina morphogenesis and cone function.

RESULTS

CRL5 expression in the developing retina

In order to address the role of CRL5 in retinal development, we first determined whether the different components of the CRL5 complex are expressed in the retina and whether their expression changes across developmental ages. We focused on the SOCS subfamily of CRL5 substrate adaptors because they have been shown to participate in the development of the CNS (Lawrenson et al., 2017; Simó and Cooper, 2013). RNA sequencing (RNA-seq) data of postnatal day (P) 15 retinas indicated that *Cul5*, *Rbx2*, *Elob* and *Eloc* (also known as *Tceb2* and *Tceb1*, respectively) are highly expressed in the retina, whereas different SOCS adaptor genes show different expression levels: SOCS1 and SOCS3 mRNAs exhibit the lowest expression levels whereas SOCS7 and SOCS5 are the most abundant SOCS mRNAs in the retina (Fig. 1B). In order to assess developmental expression changes, wild-type retinas were isolated from embryonic day (E) 13, E16, P0 and P7 mice, and subjected to RT-qPCR analyses. *Cul5* and *Rbx2* mRNAs are already detected at E13 and are continuously expressed throughout retinal development, with *Cul5* levels slightly increasing from E13 to P7 (Fig. S1). Conversely, SOCS adaptor genes are expressed at varying levels across development. *Socs5*, *Socs7* and *Cish* expression levels increase during retinal development, with *Socs7* exhibiting the highest change (Fig. S1, over a ninefold increase between E13 and P7), whereas the other SOCS family members do not exhibit significant differences across ages, suggesting that the expression of different SOCS adaptor proteins are differentially regulated during retinal development.

To gain insights into the expression pattern of *Rbx2*, we performed *in situ* hybridization at two different time-points. At E16, *Rbx2* mRNA showed high expression levels in both the neuroblastic layer (NbL) and the GCL, as well as in the developing lens, but not in the retinal pigmented epithelia or the cornea (Fig. 1C,D). In adult tissues, *Rbx2* mRNA was ubiquitously expressed in all retinal layers, with the highest levels of expression detected in the INL, and also in the epithelium and secondary lens fibers (Fig. 1H-J). *In situ* hybridization using a *Rax* probe was used as a positive control (Fig. 1G) (Furukawa et al., 1997). Together,

Development (2018) 145, dev155283. doi:10.1242/dev.155283

these results indicate that CRL5 components, including RBX2, are expressed in the developing and adult eye.

RBX2-deficient mice exhibit microphthalmia, cataracts and eyelid abnormalities

As described previously, floxed *Rbx2* mice (*Rbx2* fl/fl) crossed with Nestin-Cre (Rbx2cKO-Nes) resulted in viable but smaller animals (Fig. 2A). The Rbx2cKO-Nes mice develop progressive hydrocephalus, die around the third postnatal week, and exhibit lamination defects in the neocortex and the cerebellum (Simó and Cooper, 2013). Interestingly, Rbx2cKO-Nes mice also showed eye phenotypes with signs of eyelid ptosis presented as a significant reduction in the palpebral fissure height in both eyes as early as P15 (Fig. 2B). Because ptosis may be a secondary effect of microphthalmia, as smaller globes do not support the eyelids, we measured the size of the Rbx2cKO-Nes eyeballs in comparison with control littermates at P0. We chose P0 because at this stage there was no significant weight difference between Rbx2cKO-Nes and controls (*Rbx2* fl/fl) (Simó and Cooper, 2013). Control and Rbx2cKO-Nes eyes were dissected at P0, and axial length (anterior-posterior) and equatorial diameter (superior-inferior or nasal-temporal) were measured. A percentage of Rbx2cKO-Nes eyes were moderately smaller than the controls and, often, the observed microphthalmia was asymmetrical (Fig. 2C), suggesting that the penetrance of this phenotype might be variable and that the ptosis is not caused by the underdevelopment of the eyes because all *Rbx2* mutants exhibit eyelid defects. There were no differences in the size of the Rbx2cKO-Nes lenses compared with control littermates. However, at P15, some *Rbx2* mutant lenses showed opaque spots clustered at the core of the lens but not in the cortex (Fig. 2D). These observations indicate that RBX2 is required for proper lens transparency and that it is involved in the normal development of the eyelids and retina.

Rbx2cKO-Nes retinas accumulate DAB1 in type II amacrine cells and in the epithelium and secondary fiber cells of the lens

Given that CRL5 is expressed in the retina, we next asked whether it participates in RELN/DAB1 signaling in the developing eye. RELN is known to be expressed in several cell types of the retina, including retinal ganglion cells, amacrine cells and cone bipolar cells, whereas DAB1 expression has been proposed to be exclusive to type II (AII)-amacrine cells at postnatal ages (Rice and Curran, 2000). First, we used *in situ* hybridization to analyze the expression pattern of *Dab1* in the retina (Fig. 1E,F,K-M). We detected *Dab1* mRNA in the retina earlier than previously described (E16, Fig. 1E) and the expression persisted until late postnatal stages (P15, Fig. 1K,L). At E16, the highest expression levels of *Dab1* were detected in retinal progenitors (Fig. 1E), whereas at P15 *Dab1* mRNA was strongly detected in the inner part of the INL where AII-amacrine cells reside (Fig. 1K, arrows), in agreement with previous reports (Rice and Curran, 2000). Notably, *Dab1* mRNA was observed in a punctate distribution in other areas of the retina, particularly in the ONL and, to a lesser degree, in the GCL (Fig. 1K), as well as in the epithelium and fiber cells of the lens (Fig. 1L).

To test whether RBX2 regulates DAB1 turnover in the retina, P15 retinas from control and Rbx2cKO-Nes littermates were analyzed by western blotting (Fig. 3A-C). As expected, *Rbx2* deletion (lanes 2, 4 and 5, Fig. 3A) disrupted RBX2 expression but it also induced accumulation of DAB1. Immunoprecipitation experiments using a DAB1 antibody combined with western blot for phospho-tyrosines confirmed that, in the Rbx2cKO-Nes, DAB1 accumulates in its active, phosphorylated form (Fig. 3B). Interestingly, the tyrosine kinase FYN also accumulated in the absence of RBX2, suggesting that RBX2 controls the turnover of both DAB1 and FYN proteins in the retina (Fig. 3A-C). To identify the cells in the retina that accumulated DAB1, we performed immunofluorescence on Rbx2cKO-Nes and control retinas. DAB1 accumulated in AII-amacrine cells (Fig. 3D-E′) and, most prominently, in the distal dendrites of these cells. DAB1 also accumulated in the cytoplasm of the lens epithelium and inside the nuclei of the secondary fibers of the lens (Fig. 3F-G′). Together, these findings indicate that RBX2, most likely through CRL5 activity, regulates DAB1 and FYN turnover, and participates in the termination of RELN/DAB1 signaling in the eye.

RBX2 deficiency leads to layering defects in the retina in a DAB1-dependent and -independent fashion

We next asked whether absence of RBX2, and subsequent accumulation of pY-DAB1, altered the distribution of neurons in the retina. Depletion of RBX2 did not affect the gross morphology

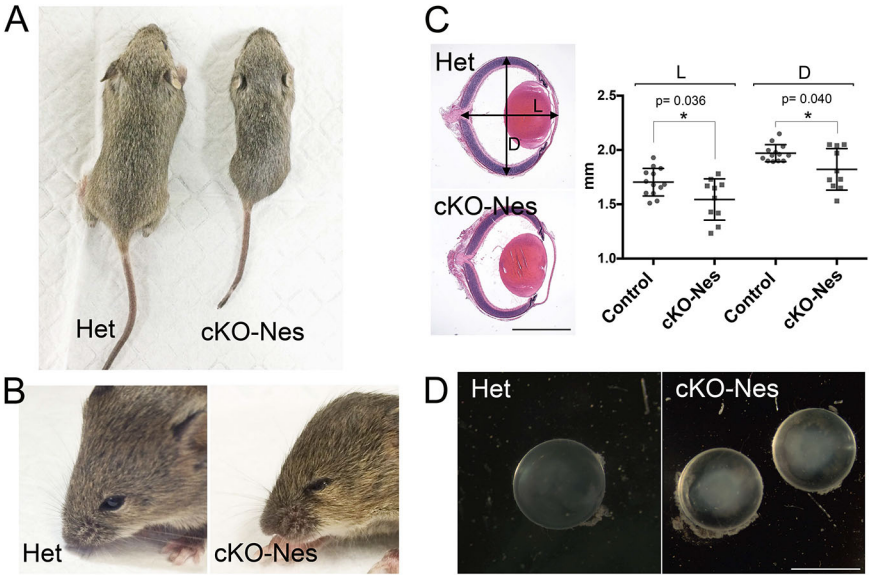

Fig. 2. Macroscopic phenotypes in Rbx2cKO-Nes mice. (A,B) Rbx2cKO-Nes mice are unable to thrive and show abnormal eye lids. Comparison between control heterozygous (Het) and Rbx2cKO-Nes (cKO-Nes) littermates at P20. (C) Rbx2cKO-Nes animals exhibit moderate microphthalmia. Comparable sagittal sections of P0 retinas stained with Hematoxylin and Eosin (left), and scatter plots of length (L, anterior-posterior) and equatorial diameter (D, nasal-temporal) measurements. Control, *n*=7; Rbx2cKO-Nes, *n*=5. (D) Rbx2cKO-Nes mice develop cataracts. Images of dissected lenses of P20 Rbx2cKO-Nes and control heterozygous littermates. Scale bars: 1 mm. *P*-values were obtained using Student's *t*-test. **P*<0.05.

Development (2018) 145, dev155283. doi:10.1242/dev.155283

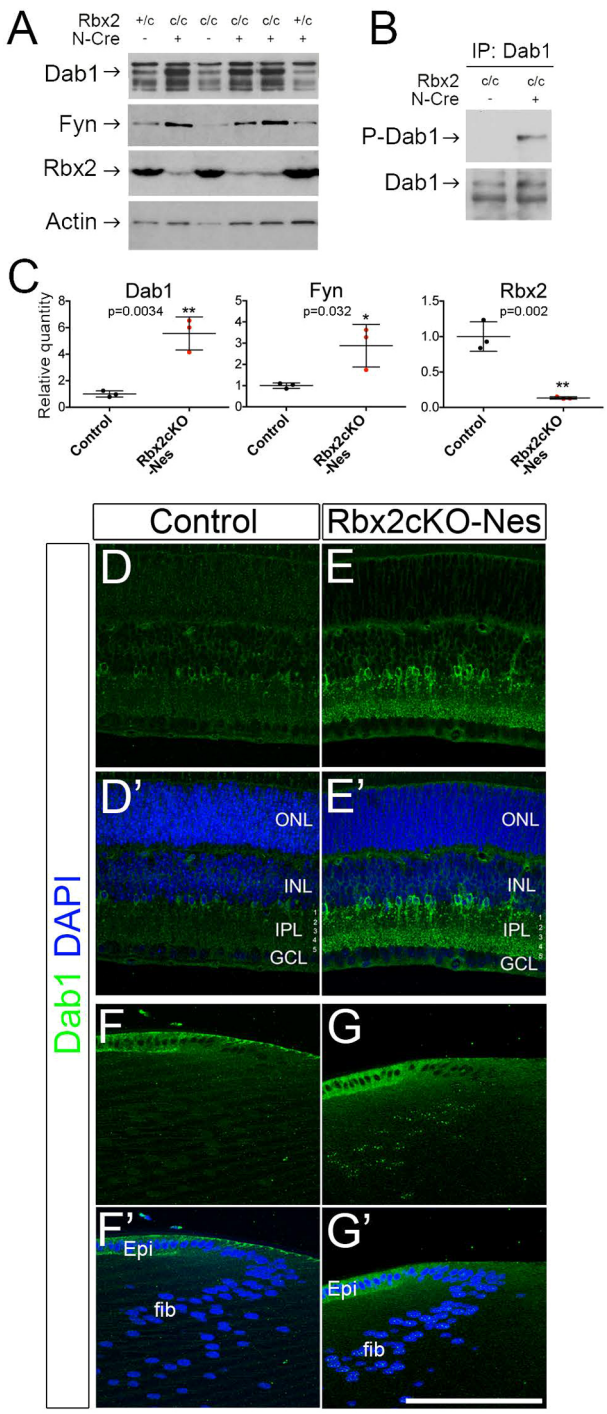

Fig. 3. RBX2 depletion inactivates CRL5 and triggers the accumulation of phosphorylated DAB1 in the retina and lenses. (A) Rbx2cKO-Nes retinas accumulate DAB1 and FYN. Western blot comparison of dissected retinas from Rbx2cKO-Nes (lanes 2, 4 and 5) and control littermates (lanes 1, 3 and 6). (B) The phosphorylation status of DAB1 was examined by immunoprecipitation experiments with DAB1 antibody followed by western blot with anti-phosphotyrosine (4G10) and total DAB1 as loading control. (C) Densitometric analyses of three independent experiments normalized to actin. Data are mean±s.d. *P* values were obtained using Student's *t*-test. **P*<0.05, ***P*<0.01. (D-G′) DAB1 accumulates in AII-amacrine cells in the retina (D-E′) and in the epithelium of the lens and lens fibers (F-G′). P15 retinal sections of Rbx2cKO-Nes and control littermates were immunolabeled with DAB1 (green) and nuclei were counterstained with DAPI (blue). ONL, outer nuclear layer; INL, inner nuclear layer; IPL, inner plexiform layer; GCL, ganglion cell layer; Epi, lens epithelium; fib, lens fibers. Scale bar: 100 µm.

of the retina and all the major retinal cell types were present. Absence of RELN or DAB1 in the retina is known to disrupt dendritogenesis of AII-amacrine cells, reduce the total number of rBCs, and alter axon elongation/stabilization of the remaining rBCs (Rice and Curran, 2000). These phenotypes may be interconnected, given that AII-amacrine cells are the postsynaptic partners of the rBCs (Hoon et al., 2014; Marc et al., 2014). Wild-type rBCs ($OTX2^+$, $PKC\alpha^+$) localize at the apical side of the INL and extend their axons to the IPL, where they establish synaptic contacts with AII-amacrine cells (Fig. 4A,A′). Absence of RBX2 resulted in rBC misplacement to the inner half of the INL at P15 (Fig. 4B,B′). Quantification of rBC distribution showed that in Rbx2cKO-Nes retinas more than 10% of rBCs were ectopically localized at the inner half of the INL in comparison with fewer than 1% in control retinas (control=0.76±1.66% versus Rbx2cKO-Nes=11.23±4.27% of cells in the inner half of the INL, Fig. 4E). In wild-type mice, by P14 rBCs have achieved their mature morphology, with apical dendrites contacting the OPL (Elshatory et al., 2007; Shen et al., 2016). Compared with the complex dendritic arbors of the cells located at the top of the INL, the displaced rBCs exhibit simpler shorter dendritic protrusions that often appear to be incorrectly polarized (arrows in Fig. 4C-D′ and Fig. S2). In contrast, the axons of the displaced rBCs do not seem to be affected; similar to the controls, all RBX2-deficient rBC axons terminate at the ON sublamina of the IPL and exhibit the characteristic polymorphic oval swellings at the axon endings (Fig. 4C-D′). Moreover, RBX2 depletion did not trigger cell death (Fig. S2D).

During normal retinal development, rBCs migrate beyond their final position towards the vitreal side of the INL to later backtrack their path to the apical side (Morgan et al., 2006). Misposition of rBCs described in Rbx2cKO-Nes retinas could be a result of inefficient backward migration or altered positioning after rBCs cells have reached their final position. In order to distinguish between these two possibilities, we collected Rbx2cKO-Nes retinas at P9, a time point when almost all wild-type rBCs have reached their final position, P15 and P21, and determined rBC localization. At P9, no significant differences were observed between Rbx2cKO-Nes and control rBCs, with most of the cells in both cases localized at the apical side of the INL (Fig. 4E), suggesting that normal rBC migration was unaffected by RBX2 depletion (control=3.07±0.61% and Rbx2cKO-Nes=7.58±2.32%). However, at later time points (P15 and P21), an increasing number of misplaced rBCs were observed (P21 control=0.725±1.35% vs P21 Rbx2cKO-Nes=16.08±5.6%, Fig. 4E), suggesting that, in *Rbx2* mutant retinas, the ectopic localization of the rBCs occurs after their normal migration period.

To assess whether accumulation of DAB1 was responsible for the phenotype observed in RBX2 mutant rBCs, we crossed Rbx2cKO-Nes mice with *Dab1* heterozygous mice (Howell et al., 1997). DAB1 accumulation in Rbx2cKO-Nes; $Dab1^{+/-}$ mice was reduced at least fourfold in comparison to Rbx2cKO-Nes mice (Simó and Cooper, 2013). Reducing DAB1 accumulation in Rbx2cKO-Nes retinas by removing one copy of *Dab1* rescued rBC displacement (Fig. 4E), indicating that DAB1 accumulation is necessary for the displacement of rBCs and further suggesting that proper termination of RELN/DAB1 signaling is crucial for rBC lamination. Next, we tested whether RBX2 depletion in rBCs was sufficient to cause rBC misposition (cell-autonomous effect), we crossed our *Rbx2* fl/fl mice with Crx-Cre mice (Rbx2cKO-Crx), in which Cre expression is restricted to bipolar and photoreceptor cells, and not present in amacrine cells (Prasov and Glaser, 2012). Rbx2cKO-Crx mice are viable and survive to adulthood. Rbx2cKO-Crx mice show a strong

Development (2018) 145, dev155283. doi:10.1242/dev.155283

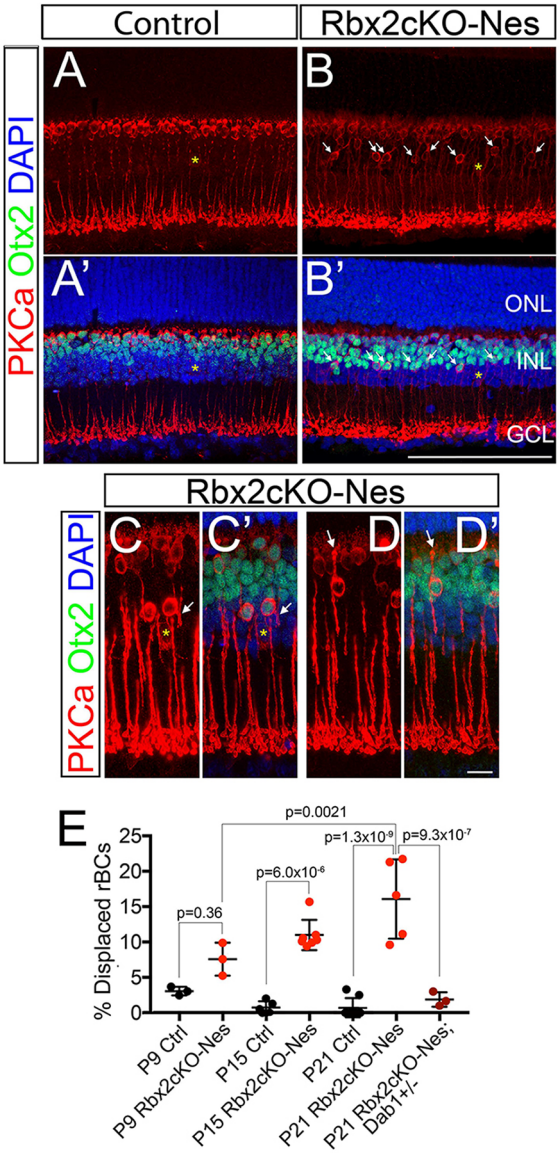

Fig. 4. Absence of RBX2 leads to abnormal rod bipolar lamination. (A-D′) Many rBCs are ectopically located in Rbx2cKO-Nes retinas. P20 control and Rbx2cKO-Nes retinas were immunostained using PKCα (red) and OTX2 (green) antibodies, and nuclei were counterstained with DAPI (blue). Note the presence of displaced PKCα$^+$ OTX2$^+$ rBCs in the Rbx2cKO-Nes samples (arrows in B,B′). (C-D′) High-magnification views of PCKα OTX2 staining revealed defects in rBC dendrites (arrows). A small fraction of PKCα$^+$ OTX2$^-$ amacrine cells were identified in some samples (yellow stars in A-C′). (E) rBC misplacement worsens over time and requires accumulation of DAB1. Quantification of the percentage of PKCα$^+$ OTX2$^+$ cells localized in the vitreal half of the INL in control mice (P9, *n*=3; P15, *n*=5; P21, *n*=7), Rbx2cKO-Nes (P9, *n*=3; P15, *n*=7; P21, *n*=5) and Rbx2cKO-Nes; *Dab1*$^{+/-}$ (P21, *n*=3). *P*-values were obtained using one-way ANOVA with Tukey's post-hoc test. ONL, outer nuclear layer; INL, inner nuclear layer; GCL, ganglion cell layer. Scale bars: 100 µm in A-B′; 15 µm in C-D′.

but incomplete decrease in RBX2 expression, consistent with Crx-specific RBX2 knockout, and did not show accumulation of DAB1 or FYN, or increased cell death (Fig. S3C-F and S2D). Immunofluorescence analyses confirmed that DAB1 levels and expression pattern in Rbx2cKO-Crx retinas were no different from the controls (Fig. S3A-B′). When we analyzed the final position of rBCs in Rbx2cKO-Crx retinas, no differences from control littermates were observed (Fig. S3G-I). Together, these data indicate that RBX2 is required to hold rBCs at the outermost part of the INL and that final rBC position is controlled through a non-cell autonomous mechanism.

RBX2 is necessary for proper position and function of cone photoreceptors

We also analyzed the cell position of other retinal populations. Although we did not detect differences in rod photoreceptors, *Rbx2* mutant cone photoreceptors were ectopically located from the outer side of the ONL, where they normally reside, to more inner positions within the ONL (Fig. 5A-C′, arrowheads). Interestingly, many of these displaced cone photoreceptors showed a disrupted outer segment and redistribution of S-Opsin towards the cell body, suggesting defects in intracellular protein trafficking (Fig. 5H,H′).

Remarkably, in the *Rbx2*-mutant retinas, we also observed cone arrestin$^+$ cells outside the ONL and, although these displaced cells often remained in the OPL, we also identified cone arrestin$^+$ cells in the INL, IPL and even in the GCL (Fig. 5C,C′, arrow). To confirm that the cone arrestin$^+$ neurons outside the ONL were cones, we co-stained Rbx2cKO-Nes retinas with cone arrestin antibodies together with antibodies against other well-known cone markers, such as OTX2 and OPN1SW (S-opsin). Displaced cone arrestin$^+$ cells were positive for OTX2 (Fig. 5D-D″) and S-Opsin (Fig. 5G-G″), confirming that these cells are indeed cone photoreceptors. To measure the extent of displacement, we measured the position of each individual cone arrestin$^+$ cell in the ONL as the ratio (x/y) of the distance from the nucleus to the top of the ONL/outer limiting membrane (x), and the thickness of the ONL in that region of the retina (y) (Fig. 5E); accordingly, a cone located at the outermost layer of the ONL would obtain an x/y value close to 0, and a cone located at the innermost side of the ONL (closer to the OPL) would obtain an x/y value close to 1. Although most cones are located at the outer side of the ONL in the control retinas (average x/y ratio=0.11±0.012, *n*=120), we observed a significant increase in the x/y ratio values in the Rbx2cKO-Nes retinas (average x/y ratio=0.1807±0.01257, *n*=167). Additionally, we counted all cone arrestin$^+$ cells outside the ONL at P20. Depletion of RBX2 significantly increased the amount of cones outside the ONL in comparison with control littermates (control=103±4.58 cells/retina versus Rbx2cKO-Nes=270±39.2 cells/retina, *n*=5 per genotype, *P*=0.000125, Student's *t*-test) (Fig. 5F). Next, we asked whether sustained RELN//DAB1 signaling was responsible for cone displacement observed in Rbx2cKO-Nes retinas. We analyzed the distribution of cones in Rbx2cKO-Nes; *Dab1*$^{+/-}$ mice and found that reduction of DAB1 levels did not rescue cone displacement (Fig. S4). Moreover, we also observed a similar cone displacement between Rbx2cKO-Crx and Rbx2cKO-Nes retinas (Fig. 6A-J), even though no DAB1 accumulation was observed in the former (Fig. S3A-D). These results indicate that RBX2 regulates cone position independently of RELN/DAB1 signaling.

To test whether RBX2 depletion affected retinal function, we used electroretinogram (ERG) recordings, which measures electrical responses of various retinal cell types, including rod and cone photoreceptors, to determine the physiological responses upon light stimulation. Given the early lethality of the Rbx2cKO-Nes mice, we used Rbx2cKO-Crx mice to perform the ERG recordings (Fig. 6). Rod-driven ERGs in response to a saturating flash were undistinguishable between wild-type and RBX2-depleted rod photoreceptors, reflecting normal rod function (Fig. 6K, Table 1). However, cone-driven ERGs in response to saturating flash showed a significant reduction of the maximal amplitudes of cone-driven b-

Development (2018) 145, dev155283. doi:10.1242/dev.155283

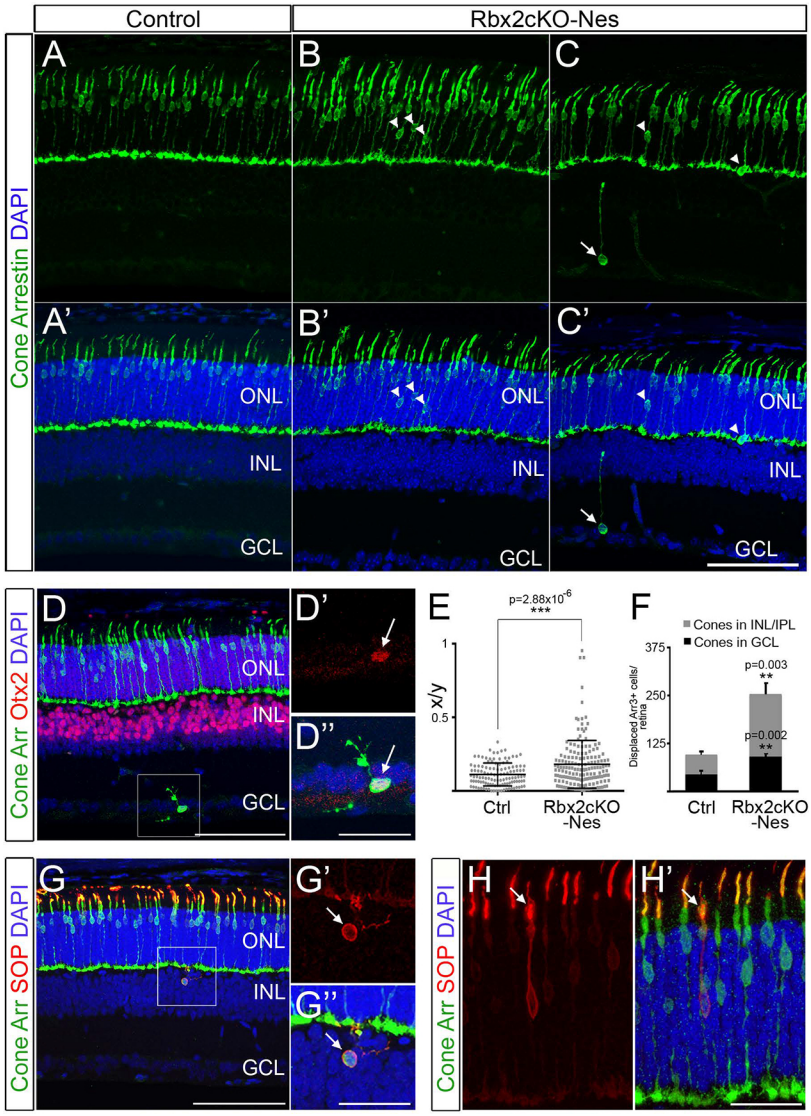

Fig. 5. RBX2-deficient retinas show cone photoreceptor defects. (A-C′) P20 retinas of control and Rbx2cKO-Nes mice labeled with antibodies against cone arrestin (green) and counterstained with DAPI (blue). Note the ectopic position of some cones in Rbx2cKO-Nes retinas (arrowheads in B-C′). Arrows in C,C′ indicate ectopic cone outside the ONL. (D-D″,G-H′) Ectopic cone arrestin$^+$ cells express other cone photoreceptor markers and show morphological defects. Control and Rbx2cKO-Nes P20 retinas were co-immunolabeled with anti-cone arrestin (green) together with anti-OTX2 (red in D-D″) or anti-S-Opsin (SOP) (red in G-H′) and counterstained with DAPI (blue). D′,D″ and G′,G″ are high-magnification views of the areas boxed in D and G, respectively. The cone arrestin$^+$ cells localized outside the ONL co-expressed OTX2 (arrows in D′,D″) and SOP (arrows in G′,G″). Many cone arrestin$^+$ cells in the ONL show a disrupted outer segment and redistribution of S-opsin towards the cell body (arrows in H,H′). (E) Scatter plot of the position of all cone nuclei obtained from three high-magnification images of different retinas (n=3 for each genotype; control=120 and Rbx2cKO=167 cone arrestin$^+$ cells). The position of each individual nucleus in the ONL was recorded as the ratio (x/y) of the distance from the nucleus to the OLM (x) and the thickness of the ONL in that region of the retina (y). (F) Quantification of cone arrestin$^+$ cells outside the ONL/OPL. Data are indicated as number of cells per retina. Control, n=3; Rbx2cKO-Nes, n=3. $^{**}P$<0.01, $^{***}P$<0.001 by Student's t-test. ONL, outer nuclear layer; INL, inner nuclear layer; GCL, ganglion cell layer. Scale bars: 100 µm in A-C′,D,G; 25 µm in D′,D″,G′,G″,H,H′.

wave (Fig. 6L,M, Table 1). Moreover, in the same context, we also observed a reduction of cone-driven a-wave, although the differences were not statistically significant (Fig. 6L,M, Table 1). To further understand the defects of RBX2 depletion, we determined the population average intensity-response function of cone-driven ERGs and found that no differences were detected between control and *Rbx2* mutants (Fig. 6N-P, Table 1). Overall, our results support reduced cone-mediated signaling in Rbx2cKO-Crx animals.

To determine how RBX2 depletion may be affecting cone function, we focused on cone pedicles, which are the synaptic terminals of cones, and used immunofluorescence against ribeye, a protein associated with ribbon synapses (Schmitz, 2009). We stained wild-type and Rbx2cKO-Nes retinas using a ribeye antibody and observed a noticeable reduction of ribeye signal in *Rbx2*-mutant retinas in comparison with their wild-type counterparts (Fig. S5A-D). To confirm the reduction of ribbon synapses, we performed electron microscopy (Fig. S5E-I). RBX2 depletion caused a decrease in the percentage of cone pedicles where ribbons could be observed (Fig. S5E,F,H), whereas rod spherules were no different between genotypes (Fig. S5E-G). Together, these data indicate that RBX2 is important for preserving proper cone location and function.

RBX2 regulates position and reactivity of Muller glial cells

MGCs are the principal glial cells of the retina. They provide mechanical support and can respond to retinal injury by changing their morphology, biochemistry, and physiology (Bringmann et al., 2006). In wild-type retinas, MGCs span across the entire thickness of the retina and have their nuclei stereotypically localized in the middle of the INL (Bringmann et al., 2006). Given that many cones were ectopically localized in Rbx2cKO-Nes mice and that alterations in the MGCs can affect the OLM and consequently, photoreceptor behavior (Shen et al., 2012; Ueki et al., 2015), we analyzed the status of the MGCs in RBX2 mutant retinas. Immunostainings against the MGC markers LHX2 and SOX2 detected foci of MGCs displaced to the OPL and even in the ONL (Fig. 7A,B and 7C′,D′). However, the general morphology of the MGCs was comparable to control retinae, including proper inner and outer processes, and endfeet structures in the inner limiting membrane (Fig. 7A′-B″). Interestingly, some displaced MGCs were positive for GFAP (Fig. 7C-D″), indicating that absence of RBX2 in the retina leads, directly or indirectly, to the expression of proteins associated with reactive gliosis. Interestingly, we also found displaced MGCs in Rbx2cKO-Nes; *Dab1*$^{+/-}$ retinas (Fig. S4B,B′, yellow arrowhead), suggesting that mislocalization of RBX2 mutant MGCs is independent of RELN/DAB1 signaling.

Development (2018) 145, dev155283. doi:10.1242/dev.155283

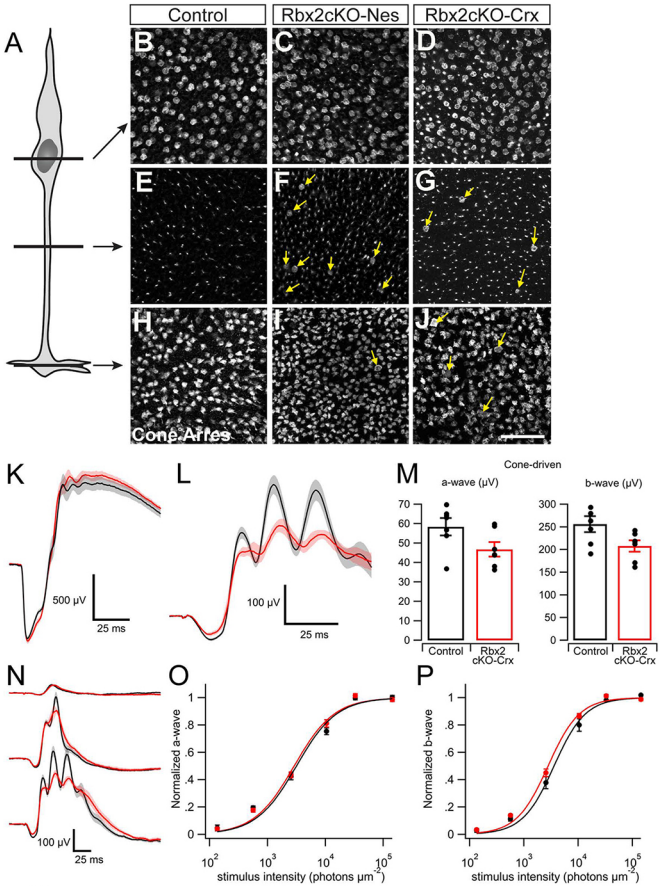

Fig. 6. Reduced cone function in Rbx2cKO-Crx mice. (A-J) P20 retinas from control (B,E,H), Rbx2cKO-Nes (C,F,I) and Rbx2cKO-Crx (D,G,J) mice were flat-mounted and immunostained using cone arrestin antibodies. (A) Pictures of the flat-mount were taken at the cone nuclear (B-D), cone axon (E-G) and cone pedicle (H-J) level. Similar to Rbx2cKO-Nes retinas, cones in Rbx2cKO-Crx retinas were found displaced throughout the ONL (F,G) and at the ONL/OPL border (I,J). Arrows indicate ectopic cone photoreceptor cell bodies. (K) Rod-driven ERGs in response to a saturating flash (3.3×10^5 photons μm^{-2}) were indistinguishable between Rbx2cKO-Crx (red) and control (black) littermates, reflecting normal rod function. (L) Cone-driven ERGs in response to a saturating flash (1.5×10^5 photons μm^{-2}) delivered on top of a rod-suppressing background (4.5×10^5 photons μm^{-2} s^{-1}) revealed that the loss of *Rbx2* expression reduced the maximal amplitudes of the cone-driven a- and b-waves by ~20%. Solid traces are population means; the shaded areas are s.e.m. (M) Individual determinations of maximal cone-driven a- and b-wave amplitudes. Data represent mean±s.e.m. for each genotype. (N) Cone-driven ERGs in response to flashes of increasing intensity (1.4×10^2-1.7×10^5 photons μm^{-2}) were used to determine population average intensity-response functions. (O,P) Normalized cone-driven a-wave intensity-response functions (O) and normalized cone-driven b-wave intensity-response functions (P) reveal no reliable difference in overall cone sensitivity. Data points are the mean±s.e.m. and were fitted by Hill functions with coefficients of 1.0 (a-waves) and 1.5 (b-waves). *n*=7 animals per genotype (K-P) Scale bars: 30 μm.

In several human retinopathies, loss of MGCs alters homeostasis and survival of photoreceptors, and, similarly, loss of photoreceptors activates MGCs (Bringmann et al., 2006). We further assessed whether the cone and MGC phenotypes were geographically correlated. Although, in some cases, foci of reactive MGCs were in the same area as displaced cones, this was not a generalized observation and we were not able to conclude that displaced MGCs affect cone location or vice versa.

CRL5 uses the substrate adaptor SOCS7 to regulate rod bipolar cell and Muller glia cell positioning

Finally, to determine whether pY-DAB1 accumulation is sufficient to induce retinal cell displacement, we analyzed the retinal lamination and morphology of *Socs7* mutant retinas. In these animals, only the turnover of SOCS7-CRL5-specific substrates is affected. Thus, depletion of SOCS7 can induce accumulation of pY-DAB1 without affecting the overall CRL5 activity. As expected, pY-DAB1 accumulated in the absence of SOCS7 but, interestingly, we did not observe a similar accumulation of FYN (Fig. 8A,B). DAB1 accumulation in *Socs7* mutant retinas was detected mainly in AII-amacrine cells (Fig. 8C-D′). Despite the observation that pY-DAB1 accumulated at similar levels to those seen in Rbx2cKO-Nes retinas (Fig. 3C), rBC localization in *Socs7* mutant mice was affected to a lesser degree (Fig. 8G, Rbx2cKO-Nes=11.23±4.27% vs *Socs7* KO=4.01±2.43%). These results suggest that other SOCS7-independent RBX2-dependent substrates are involved in rBCs localization besides DAB1. Next, we analyzed the localization of cone photoreceptors and MGCs in *Socs7* mutants. Whereas localization of cone photoreceptors was not disrupted in the absence of SOCS7 (Fig. 8I), some MGCs were displaced towards the ONL and showed signs of gliosis, as previously observed in Rbx2cKO-Nes mice (Fig. 8E-F′,H). Overall, these results indicate that SOCS7-CRL5 regulates the proper localization of both rBCs and MGCs, and further suggest that CRL5 control rBC positioning through the regulation of multiple proteins, including DAB1 (Fig. 9).

DISCUSSION

Retina morphogenesis requires the timely activation of a myriad of signaling pathways (Carl and Wittbrodt, 1999; Close et al., 2006; Dakubo et al., 2003; Hernández-Bejarano et al., 2015; Maurer et al., 2014; Nelson et al., 2007; Roberts et al., 2006; Ueki and Reh, 2013). Whereas much progress has been made in understanding the molecular mechanisms that regulate retinal synaptogenesis (Morgan and Wong, 1995; Nguyen-Ba-Charvet and Chedotal, 2014; Robles and Baier, 2012), only a handful of proteins have been shown to regulate retinal cell migration (Jimeno et al., 2016; Krol et al., 2016; Malicki et al., 2003; Matsunaga et al., 1988). Furthermore, the importance of signal termination for proper retina development and the molecular players involved in this process have not been addressed.

Our results show that RBX2, a core component of the E3 ubiquitin ligase CRL5, is required for proper cell positioning and cone function in mice. Upon RBX2 depletion in the retina, a subset of rBCs, cones and MGCs are ectopically localized. Inhibition of RBX2, most likely through CRL5 activity, also promotes accumulation of the intracellular adaptor DAB1 in AII-amacrine cells. Our data indicate that the accumulation of activated DAB1 (pY-DAB1) in AII-amacrine is necessary for rBC misplacement, as a genetic reduction of DAB1 levels ameliorates RBX2 depletion. However, depletion of RBX2 in bipolar cells using Crx as a Cre driver is not sufficient to cause the rBC displacement. This suggests that the final localization of rBCs may be regulated non-cell-autonomously through AII-amacrine cells.

Interestingly, depletion of the CRL5 substrate adaptor SOCS7 also triggers accumulation of DAB1 in AII-amacrine cells but, in these mutants, significantly fewer rBCs are affected, indicating that deregulation of other RBX2-dependent signaling pathways is necessary to alter rBC localization and that DAB1 accumulation is necessary but not sufficient. RBX2 is also crucial for cone localization, structure and activity. Absence of RBX2, but not SOCS7, promotes cone displacement from the apical side of the ONL to its inner side, and even outside the ONL. Depletion of

Development (2018) 145, dev155283. doi:10.1242/dev.155283

Table 1. ERG characteristics of Rbx2cKO-Crx and control littermates

	a-wave maximum (μV)	b-wave maximum (μV)	I_o a-wave (photons μm^{-2})	I_o b-wave (photons μm^{-2})
Wild-type scotopic	830±24	1831±105	-	-
Mutant scotopic	867±27	1908±88	-	-
P	0.29	0.55	-	-
Wild-type photopic	58±4	256±18	3287±379	3855±502
Mutant photopic	47±4	208±12	2746±354	2812±218
P	0.05	0.03	0.28	0.06

I_o corresponds to the half-saturating flash strength of the intensity-response functions. Data represent mean±s.e.m. *P* values were obtained using Student's *t*-test. *n*=7 animals per genotype.
- indicates not applicable.

RBX2 affects the amount of the structural protein RIBEYE in RBX2 mutant retinas, which could be responsible for the decreased cone functional response in ERG assays. Finally, lack of RBX2 or SOCS7, most likely clustered in the SOCS7-CRL5 complex, result in MGC positioning defects and upregulation of proteins related to glial reactivity. In summary, our data indicate that RBX2 is important for restricting neuron migration and building functional cone pedicles by terminating different signaling pathways in different retinal cell populations.

Role of RELN/DAB1 signaling in the retina

Previous studies have addressed the role of RELN and DAB1 during retinal development in several species, particularly in mice and chickens (Gao et al., 2010; Katyal et al., 2011; Rice and Curran, 2000; Rice et al., 2001). These studies showed that mutations of RELN or DAB1 disrupt AII-amacrine dendritogenesis affecting the axons of rBCs and inducing rBC death (Rice et al., 2001). Otherwise, absence of RELN/DAB1 signaling does not disrupt retina layering or neuron positioning, contrasting with the severe *Reln* or *Dab1* mutant phenotypes in other areas of the CNS (Boyle et al., 2011; Howell et al., 1997; Rice et al., 2001; Tissir and Goffinet, 2003). A retina-specific *Dab1* isoform (DAB1-E), unable to respond to RELN, is expressed in the early retina, impeding early differentiation of neural progenitors into RGCs (Gao et al., 2010). Given that DAB1-E does not respond to RELN and that our results indicate that RBX2, most likely through CRL5 activity, controls neuron position through the canonical DAB1 isoform, we do not expect that phenotypes observed in Rbx2cKO-Nes retinas depend on disruption of DAB1-E activity. The relationship between other DAB1 isoforms and CRL5 remain to be tested (Gao and Godbout, 2013). pY-DAB1 accumulation in AII-amacrines is necessary for the rBC displacement phenotype but the differences in rBC displacement observed between Rbx2cKO-Nes and SOCS7 KO mice suggest that other molecular players affected by RBX2 depletion also control rBC localization. One possible candidate is the tyrosine kinase FYN, which accumulates in Rbx2cKO-Nes but not in SOCS7 mutant mice. Our data substantiate the hypothesis that the appropriate termination of the RELN/DAB1 signaling pathway is crucial for both retina and overall CNS development.

How might extra RELN/DAB1 signaling promote rBC misplacement? Time-lapse experiments have shown that, after birth, rBCs initially use a somal translocation-like mode of migration to reach the innermost side of the INL and later migrate back to their final position at the outermost side of the INL (Chow et al., 2015; Morgan et al., 2006). Our data show that rBC initial migration mimics wild-type cells and that displacement occurs at the time where wild-type rBCs have stopped migration. In the cortex, somal translocation is the final step in projection neuron migration and is regulated by RELN/DAB1 signaling (Franco et al., 2011; Nadarajah et al., 2001). Sustained RELN/DAB1 signaling in cortical neurons causes an over-migration phenotype by extending somal translocation for longer periods of time (Feng et al., 2007; Simo et al., 2010). In this context, two possibilities could explain the rBC mispositioning observed in Rbx2cKO-Nes and SOCS7 KO mice: (1) depletion of RBX2 fails to terminate pro-migratory signals, including RELN/DAB1 signaling, that re-activate migration of rBCs that have already reached their final position at the outermost side of the INL; or (2) sustained RELN/DAB1 signaling disrupts the stereotypical rBC dendritic tree, causing a lack of tension at the apical side of the rBCs and resulting in activation of a spring-like mechanism, previously described in somal translocating cortical neurons, hence displacing the rBCs from their normal position (Miyata and Ogawa, 2007). Independent of the mechanism responsible for localizing and holding rBCs at the outermost side of the INL, our data indicate that this process is controlled in by a non-cell-autonomous signaling pathway that is directed, most likely, by the AII-amacrine cells. The nature of such signaling pathways will require further investigation.

RBX2 and cone photoreceptor localization and function

Few studies have addressed the molecular mechanisms that regulate cone localization in the ONL. For example, mutation of the guanine nucleotide exchange factor rasGRF2 displaced cones beyond the outer limiting membrane, and disruption of the linkers of the nucleoskeleton to the cytoskeleton (LINC) complexes displaces cones to the basal side of the ONL (Jimeno et al., 2016; Razafsky et al., 2012). In addition, mouse models of photoreceptor neurodegeneration, including rd1 (rod) and cpfl1 (cone), exhibit cone mispositioning as neurodegeneration progresses (Chang et al., 2009; Trifunović et al., 2010). Our results are in line with a role of RBX2 in directly regulating cone position rather than cone misplacement being a secondary effect of neurodegeneration. Given the complex migration behaviors followed by cones during development (Poggi et al., 2005; Rich et al., 1997), further studies will be needed to address whether the defects observed in RBX2 mutant retinas originate during initial cone migration or, similar to rBCs, whether cones 're-engage' migration after reaching their intended locations. Our results also indicate a role for RBX2 in synaptic ribbon establishment or maintenance, which could be related to the functional impairment observed in Rbx2cKO-Crx retinas. Whether synaptogenesis is disrupted by misposition of the cone nuclei (Razafsky et al., 2012) or conversely lack of proper synaptic establishment affects cone position in *Rbx2* mutant retinas remains to be determined.

RBX2 and human chromosome 3 deletions

In humans, a rare interstitial deletion in the long arm of chromosome 3 (3q22-q23 microdeletion) causes ptosis, microphthalmia, developmental delays and brain malformation, among other phenotypes (Al-Awadi et al., 1986; Alvarado et al., 1987; Martsolf and Ray, 1983; Rea et al., 2010; Zahanova et al., 2012). These

Development (2018) 145, dev155283. doi:10.1242/dev.155283

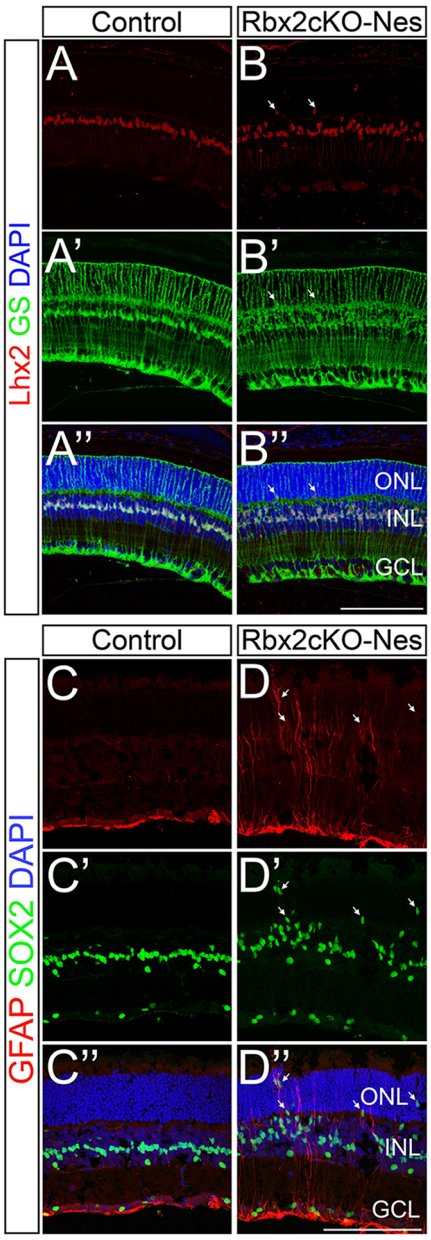

Fig. 7. RBX2 depletion leads to reactive gliosis and Muller glia layering defects. (A-B″) P20 retinas from control and Rbx2cKO-Nes littermates were immunostained using antibodies to LHX2 (red) and glutamine synthetase (GS, green), and counterstained with DAPI (blue). $LHX2^{+}$ GS^{+} cells are present in the ONL (arrows in B-B″). (C-D″) Retinas from P20 control and Rbx2cKO-Nes mice stained using anti-glial fibrillary acidic protein (GFAP, red) and anti-SOX2 (green), and counterstained with DAPI. Depletion of RBX2 leads to glial reactivity (arrows in D-D″). ONL, outer nuclear layer; INL, inner nuclear layer; GCL, ganglion cell layer. Scale bars: 100 µm.

symptoms bear a strong resemblance to the phenotypes observed in Rbx2cKO-Nes mice. The eye phenotypes in these individuals have been linked to the well-studied blepharophimosis, ptosis and epicanthus inversus syndrome (BPES, OMIM #110100), which is caused by mutations in the forkhead transcription factor gene *FOXL2* (De Baere et al., 2001). In some cases, *de novo* deletions in chromosome 3 do not include *FOXL2*, but BPES-like phenotypes remain present (Beysen et al., 2005; Rea et al., 2010). The authors of these studies have suggested that potentially long-range cis-regulatory elements might be deleted in these cases, affecting *FOXL2* expression (Beysen et al., 2005; Rea et al., 2010). Interestingly, in humans, *RBX2* is localized in the vicinity of *FOXL2* and is deleted in the Rea et al. study, which includes five previously described cases of *RBX2* but not *FOXL2* deletions, all presenting phenotypes resembling those observed in Rbx2cKO-Nes mice (Rea et al., 2010). Given that Rbx2cKO-Nes animals have a mutation that specifically targets the exon 2 of *Rbx2* with no defects on *FOXL2* expression (Simó and Cooper, 2013), our results suggest that deletion of *RBX2* may participate in some of the human eye phenotypes of 3q22-q23 deletions, including ptosis and microphthalmia.

MATERIALS AND METHODS

Mice

Rbx2 fl/fl mice (*Mus musculus*) were crossed with *Rbx2* fl/+; Nestin-Cre/+ to generate Rbx2cKO-Nes animals, as described previously (Simó and Cooper, 2013). *Dab1* heterozygous animals (Howell et al., 1997) were crossed with *Rbx2* fl/+; Nestin-Cre/+ to obtain *Rbx2* fl/+; Nestin-Cre/+; *Dab1* +/−, which were further crossed with *Rbx2* fl/fl to obtain Rbx2cKO-Nes; $Dab1^{+/-}$ mice. A similar strategy was used to generate *Rbx2* fl/fl; Crx-Cre/+ mice (Crx-Cre mice were generously provided by Dr Nadean Brown and Dr Tom Glaser, University of California Davis, USA) (Prasov and Glaser, 2012). *Socs7* KO mice were obtained from *Socs7* fl/fl mice (Simó and Cooper, 2013) crossed with Meox2-Cre mice (Tallquist and Soriano, 2000). *Sics7* fl/fl; Meox2-Cre/+ mice were further mated to wild-type C57BL6 mice (Charles River) and *Socs7* heterozygous mutant animals (without the Meox2-Cre allele) were selected for colony propagation. Heterozygous *Socs7* intercrossings were used to generate *Socs7* mutant animals and littermate controls. *Socs7* mutant mice were viable and fertile. *Rbx2* and *Socs7* LacZ animals have been previously described (Simó and Cooper, 2013). All our strains are maintained in a mix of 129 and C57Bl/6J backgrounds. The morning a vaginal plug was observed was considered E0. All animals were used with approval from the University of California Davis Institutional Animal Care and Use Committees.

Next generation sequencing

Strand-specific and barcode-indexed RNA-seq libraries were generated from 1 µg total RNA each after poly-A enrichment using the Kapa Stranded mRNA-seq kit (KapaBiosystems) following manufacturer instructions. Libraries were analyzed with a Bioanalyzer 2100 instrument (Agilent), quantified by fluorometry on a Qubit instrument (LifeTechnologies) and pooled in equimolar ratios. The pool was quantified by qPCR with a Kapa Library Quant kit (KapaBiosystems) and sequenced on one high output flowcell of an Illumina NextSeq 500 (Illumina) with paired-end 40 bp reads.

RNA analyses

Total RNA from wild-type E13, E16, P0 and P7 mouse retinas was isolated using Trizol (Invitrogen). cDNA was obtained by reverse transcription using the iSCRIPT system (Bio-Rad). Transcripts of interest were quantified by real-time PCR using gene-specific primers and the iTaq Universal SYBR Green Supermix (Bio-Rad). Data were normalized to the mean of *Gapdh* and β-actin RNA levels. The ΔΔCt method was used to compare all the samples with their E13 mRNA levels, which was standardized to 1.

Primers used were: β-actin, 5′-CTAAGGCCAACCGTGAAAAG-3′ and 5′-ACCAGAGGCATACAGGGACA-3′; GAPDH, 5′-TGACCACAGTCCATGCCATC-3′ and 5′-GACGGACACATTGGGGGTAG-3′; Cul5, 5′-TCCGATACTTAGAAACACGACGA-3′ and 5′-TGCCTTGGCATTCTGCTAAAATA-3′; Rbx2, 5′-ACCCTGCGTCCTTTCTTCG-3′ and 5′-GGCACAGGTATCGCACTCAA-3′; SOCS1, 5′-CTGCGGCTTCTATTGGGGAC-3′ and 5′-AAAAGGCAGTCGAAGGTCTCG-3′; SOCS2, 5′-GTGGGGAACTCGTCCTATCTG-3′ and 5′-GTCACAGTGTAATGATGTGCC-3′; SOCS3, 5′-ATGGTCACCCACAGCAAGTTT-3′ and 5′-TCCAGTAGAATCCGCTCTCCT-3′; SOCS4, 5′-CGGAGTCGAAGTGCTGACAG-3′ and 5′-ACTCAATGGACGAACAGCTAAG-3′; SOCS5, 5′-GAGGGAGGAAGCCGTAATGAG-3′ and 5′-CGGCACAGTTTTGGTTCCG-3′; SOCS6, 5′-AAGCAAAGACGAAACTGAGTTCA-3′ and 5′-CGCTGCCAATGTCACAACTG-3′; SOCS7, 5′-TCAGTCGCCT

Development (2018) 145, dev155283. doi:10.1242/dev.155283

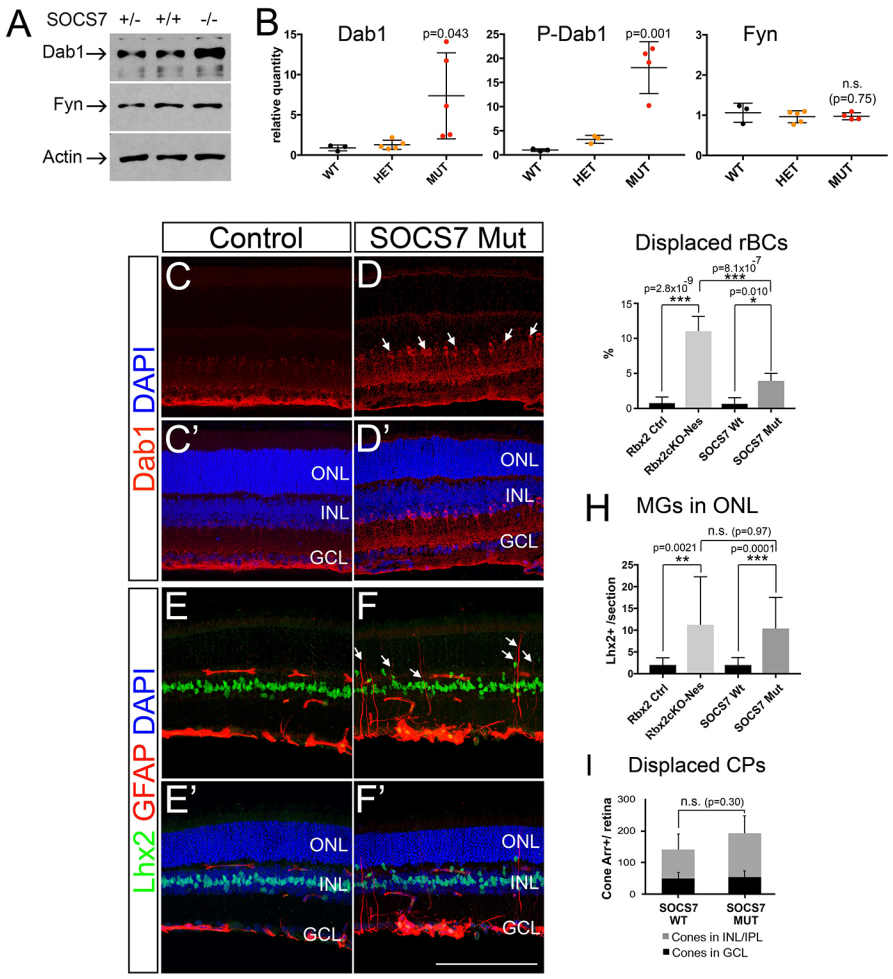

Fig. 8. *Socs7* mutant retinas accumulate pY-DAB1 and display some layering defects. (A) *Socs7* KO retinas accumulate DAB1 but not FYN. Western blot comparison of retina lysates from wild-type (+/+), *Socs7* heterozygous (+/–) and *Socs7* KO (–/–) littermates. (B) Densitometric analyses of independent experiments normalized to actin. Data are mean±s.d. *P*-values were obtained by one-way ANOVA with Tukey's post-hoc test. (C-D′) DAB1 accumulates in AII-amacrine cells in *Socs7* mutant retinas. P15 retinal sections of *Socs7* KO and control littermates were immunolabeled using anti-DAB1 (red) and nuclei were counterstained with DAPI (blue). (E-F′) Muller glial cell (MGC) mislocalization and gliosis in *Socs7* mutants. P20 retinas were co-immunostained using anti-LHX2 (green) and anti-GFAP (red), and DAPI (blue) was used to stain all the nuclei. Upregulated GFAP expression in MGCs indicates reactive gliosis (arrows in F). (G) Quantification of the percentage of PKCα$^+$ OTX2$^+$ cells localized in the inner half of the INL in wild-type and *Socs7* KO mice (*n*=5 per genotype) in P20 retinas. Same Rbx2 data as in Fig. 4E has been used for comparison. (H) Quantification of LHX2$^+$ cells in the ONL in P20 control and Rbx2cKO-Nes littermates and P20 *Socs7* wild-type and mutant retinas (*n*=5 per genotype). (I) Quantification of cone arrestin$^+$ cells outside the ONL/OPL. Data are indicated as mean number of cells per retina±s.d. (*n*=3 per genotype). *P* values were obtained using one-way ANOVA with Tukey's post-hoc test and Student's *t*-test. **P*<0.05, ***P*<0.01, ****P*<0.001. ONL, outer nuclear layer; INL, inner nuclear layer; GCL, ganglion cell layer; CPs, cone photoreceptors; n.s., non-significant. Scale bar: 100 µm.

GTTTCGCAC-3′ and 5′-GTTTCCTCCCCGTATCCAGC-3′; CISH, 5′-ATGGTCCTTTGCGTACAGGG-3′ and 5′-GGAATGCCCCAGTGGGTAAG-3′.

Antibodies

The following antibodies were used for biochemistry: rabbit anti-DAB1 (EMD Millipore Cat#AB5840), 1:1000; rabbit anti-DAB1 (Rockland Cat#100-401-225), 1:5000; goat anti-DAB1 (E-19, Santa Cruz Biotechnology Cat#SC-7827), 1:1000; rabbit anti-Rbx2 (G-8, Santa Cruz Biotechnology Cat#SC-166554), 1:1000; rabbit anti-FYN (FYN3, Santa Cruz Biotechnology Cat#SC-16), 1:1000; goat anti-actin (I-19) (Santa Cruz Biotechnology Cat#SC-1616), 1:20,000; and mouse anti-phosphotyrosine (4G10. Millipore Cat#05-321), 1:5000.

The following antibodies were used for immunofluorescence: rabbit anti-DAB1 (EMD Millipore Cat#AB5840. Discontinued), 1:100; rabbit anti-DAB1 (Sigma-Aldrich Cat#HPA052033), 1:100; rabbit anti-cone arrestin (Millipore Cat#AB15282), 1:10,000; mouse anti-protein kinase C α (Sigma-Aldrich Cat#P5704), 1:200; goat anti-blue cone opsin/OPN1SW (N-20 Santa Cruz Biotechnology Cat#14363), 1:200; goat anti-LHX2 (C-20 Santa Cruz Biotechnology Cat#SC-19344), 1:200; mouse anti-glutamine synthetase (clone GS-6, Millipore Cat#MAB302), 1:300; goat anti-OTX2 (R&D Systems, Cat#BAF1979), 1:500; mouse anti-GFAP (clone N206A/8, NeuroMAb Cat#73-240), 1:2 (supernatant); rabbit anti-RCAS1 (clone D2B6N, Cell Signaling Technology, #12290T), 1:200; rabbit anti-activated caspase 3 (Cell Signaling Technology, #9664S), 1:200; and rabbit anti-RIBEYE (Synaptic Systems #192103), 1:200. See Table S1 for authentication methods.

Western blot

For immunoblotting of retinal lysates, retinal samples were dissected in ice-cold PBS and snap-frozen in liquid N_2. Tissues were homogenized in lysis buffer [50 mM HEPES (pH 7.5), 150 mM NaCl, 1.5 mM EGTA, 10% glycerol, 1% Triton X-100, 2 mM PMSF, 10 µg/ml leupeptin, 1 µg/ml aprotinin, 10 mM NaF and 1 mM orthovanadate] on ice and clarified by centrifugation at 4°C for 15 min. Western blotting was carried out using standard protocols described elsewhere (Simo et al., 2010).

Immunoprecipitation

Retinal lysates were incubated with DAB1 antibodies (Santa Cruz Biotechnology) for 3 h at 4°C with agitation. DAB1 was immobilized on Protein A/G beads by incubating for 1 h at 4°C with agitation. Next, beads were washed with lysis buffer five times and analyzed by SDS-PAGE and western blot.

Histology

For cryosection samples, pups were recovered at P15 or P21, eyes dissected and lenses removed prior to 4% PFA fixation for 30-60 min at room temperature. Samples were cryoprotected with 30% sucrose, embedded in OCT (Fisherbrand) and quickly frozen using dry ice. For immunofluorescence studies, cryosections were blocked in 10% normal goat serum/0.5% Triton X-100 in PBS for 1 h and incubated overnight at 4°C with primary antibodies in the same solution. For paraffin samples, eyes were collected and frozen in dry-ice chilled propane then freeze-substituted with methanol-acetic acid at −80°C, as described previously (Sun et al., 2015), transferred to ethanol and embedded in paraffin wax. Paraffin wax-embedded sections were deparaffinized using Xylene and rehydrated, and immunofluorescence studies proceeded as described previously (Simó and Cooper, 2013). In both cases, after primary antibody incubation, sections were rinsed in PBS-0.1% Triton X-100 and incubated with appropriate fluorescence-conjugated secondary antibodies (Invitrogen) in blocking solution for 1 h at room temperature. Cell nuclei were counterstained with DAPI. The sections were

Development (2018) 145, dev155283. doi:10.1242/dev.155283

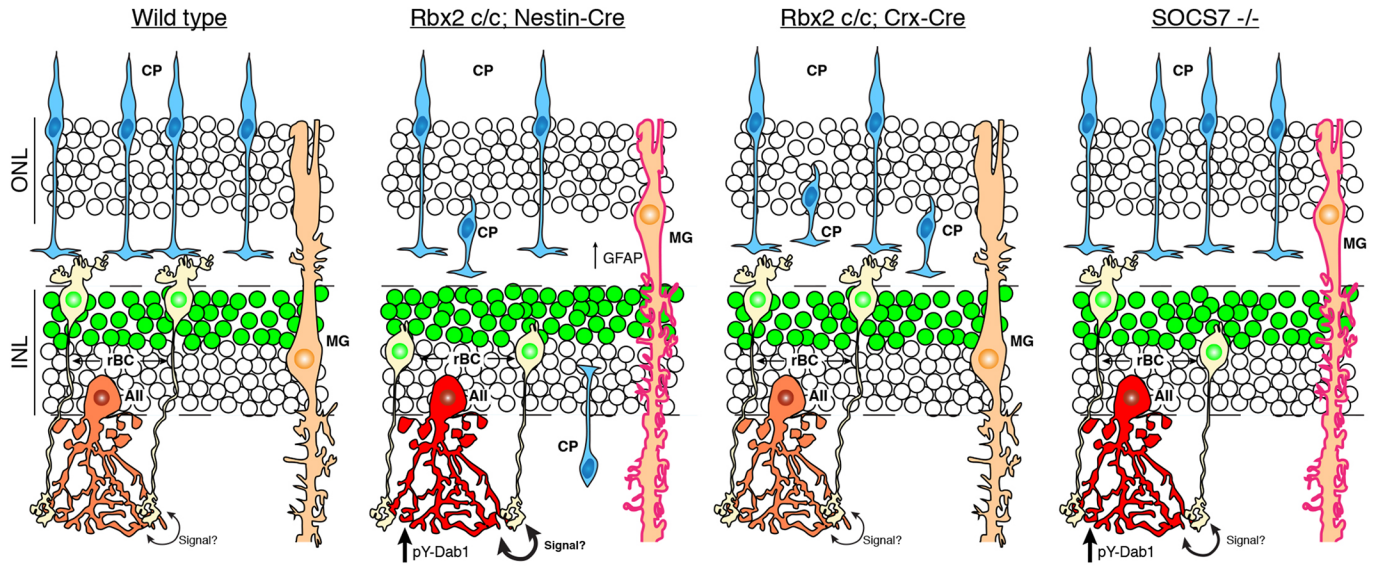

Fig. 9. Schematic diagram of the phenotypes observed in wild-type, Rbx2cKO-Nes, Rbx2cKO-Crx and *Socs7* mutant retinas. Compared with the normal P20 wild-type retinas, Rbx2cKO-Nes mice show accumulation of active pY-DAB1 (red in AII cells) in AII-amacrine cells, displacement of rBCs, cones (CPs) and Muller glia (MG), and signs of reactive gliosis (increased expression of GFAP, red in MG). In contrast, Rbx2cKO-Crx mice, where Rbx2 is depleted exclusively in photoreceptors and bipolar cells, do not show defects in DAB1 turnover or rBC and MG position. However, displaced cones are found in Rbx2cKO-Crx retinas. *Socs7* mutants also accumulate pY-DAB1 in AII-amacrine cells but the rBC phenotype is significantly reduced. Cones do not show any alteration compared with wild-type retinas but MGs are displaced towards the ONL and exhibit reactive changes, similar to the Rbx2cKO-Nes. Double-headed arrows indicate a potential non-cell-autonomous control of rBC localization by AII-amacrine cells. This 'signal' (double-headed arrows) may be stronger in Rbx2cKO-Nes (thicker lines) than in *Socs7* KO retinas affecting a greater number of rBCs.

rinsed with PBS-0.1% Triton X-100 and mounted for microscopy using a Fluoromount-G (Southern Biotech).

Most images were obtained with a 40× oil objective and captured with an Olympus FV1000 confocal microscope. High-magnification images were obtained with a 63× oil objective. Images were assembled in Adobe Photoshop and Illustrator. Brightness and contrast were similarly adjusted to all samples.

In situ hybridization

Embryos were collected from pregnant CD-1 females (Charles River) at E16 and whole heads were fixed in a modified Carnoy's fixative overnight at 4°C. Whole eyes were collected at P15 from CD-1 mice and fixed in a modified Carnoy's fixative overnight at 4°C. After fixation, samples were dehydrated in 100% ethanol overnight at 4°C and embedded in paraffin wax. Horizontal sections of whole embryo heads or sagittal sections of whole eyes were prepared at 7 µm, collected onto SuperFrost slides and air-dried overnight at room temperature. A digoxigenin (DIG)-labeled probe for mouse *Dab1* was produced according to manufacturer's protocol (Roche). Slides were deparaffinized and hybridized with 2 µg *Dab1* antisense or sense probes, as previously described (Hayashi et al., 2007). The *in situ* hybridization product was visualized using an alkaline phosphatase-conjugated anti-dig secondary antibody (Roche) and NBT (nitroblue tetrazolium)/BCIP (5-bromo-4-chloro-3-indolyl phosphate) stock solution (Roche). After the reaction was complete, slides were fixed in 4% paraformaldehyde and coverslipped with Fluoromount G (Southern Biotech). The plasmid used to produce a DIG-labeled probe was a gift from Dr Jonathan A. Cooper (Fred Hutchinson Cancer Center, Seattle, WA, USA) and corresponds to nucleotides 316-1982 of mouse *Dab1* mRNA, transcript variant 2 (NM_177259.4) cloned into pBSII-KS(+). Antisense *Dab1* probe was produced by linearizing with *Not*I and transcribing with T3 RNA polymerase. A corresponding sense probe was produced by linearizing with *Sal*I and transcribing with T7 RNA polymerase. We do not expect that this probe would distinguish between the known *Dab1* splice variants (Gao et al., 2010). Antisense Rbx2 probe corresponds to nucleotides 117-1137 of mouse *Rbx2* mRNA, transcript variant 1 (NM_011279.3) cloned into pCR-Blunt II-TOPO (Invitrogen). Antisense *Rbx2* probe was produced by linearizing with *Kpn*I and transcribing with T7 RNA polymerase. A corresponding sense probe was produced by linearizing with *Not*I and transcribing with SP6 RNA polymerase. Sense and antisense images were captured at same exposure time. Most images were obtained with a 10× and 20× objective, and captured with Zeiss AxioImager software. Images were assembled in Adobe Photoshop and Adobe Illustrator.

Electroretinogram recordings

Young adult *Rbx2* mutant and wild-type littermate mice were dark adapted overnight before recording. Under dim red light, animals were anesthetized with isofluorane (1.5%) and positioned on a regulated heating pad that maintained a core temperature of 37°C. A mixture of phenylephrine and tropicamide was applied to the corneal surface to achieve mydriasis and induce proptosis, increasing the electrical resistance between the surface of the cornea and the rest of the body. Methylcellulose was applied to maintain corneal moisture during the recording.

A Ganzfeld ERG system (Phoenix Research Labs) was used for light stimulation (510 nm LED, 1 ms flashes) and electrical recording, as described by Peinado et al. (2017). The total number of photons generated for all stimuli were measured using a high-speed photodiode (UDT Instruments) and calibrated neutral density filters. Isolation of cone-elicited signals was achieved by superimposing flashes to a rod-suppressing background intensity of 45,000 photons μm^{-2} s^{-1}.

Electrical responses were acquired with the Labscribe2ERG interface (Phoenix Research Labs) and subsequently exported to Igor Pro (WaveMetrics) for analysis. For all ERG responses, the amplitude of the a-waves was measured from baseline to peak of the negative excursion, which followed flash delivery. Scotopic (rod-driven, dark-adapted) b-wave amplitudes were measured from the peak of the a-wave to the first peak of the positive-going excursion. The oscillatory potentials of photopic b-waves were removed prior to determining the peak amplitudes using a sliding average algorithm (2500 passes of IgorPro binomial smoothing built-in algorithm). The amplitude of the photopic b-wave was measured from baseline to the peak of the smoothed b-wave. Intensity-response functions for photopic (cone-driven) a-waves and b-waves were fitted by a Hill equation of the form , where R is the amplitude of the elicited response, R_{max} is the maximal response amplitude, I is the flash strength, I_o is the flash

Development (2018) 145, dev155283. doi:10.1242/dev.155283

strength that elicits a half-maximal response and n is the Hill coefficient. For a-wave intensity-$R/R_{max} = 1/\left[1 + \left(\frac{I_o}{I}\right)^n\right]$response functions, n was held fixed at a value of 1. For b-wave intensity-response functions, n was held fixed at a value of 1.5.

Electron microscopy

Tissues were fixed by immersion in 2% glutaraldehyde and 2.5% formaldehyde in 0.1 M cacodylate buffer (pH 7.4) for 12 h at room temperature. Eyes were opened and a region of the posterior eye cup adjacent to the optic nerve head was dissected free. Tissue was rinsed with cacodylate buffer and then post-fixed with 2% osmium tetraoxide for 1 h. After a water rinse, tissues were dehydrated through 10 min exchanges of 70%, 80%, 90% and 100% ethanol. After a second 100% ethanol rinse, ethanol was exchanged for propylene oxide using two 10 min washes. Tissues were then immersed in 1:1 propylene oxide:Polybed 812 (Polysciences) for 12 h. Tissues were then moved into 100% Polybed 812 for 2 h, followed by polymerization overnight for 24 h at 60°C. Sections were stained sequentially with uranyl acetate and lead citrate, and imaged on a Talos L120C at 80 kV, using the CETA digital camera.

Experimental design and statistical analysis

Complete results of statistical analyses are reported in figure legends. All cell measurements and densitometry were carried out using ImageJ software (NIH), and all statistical analyses were performed using Prism 7 software (GraphPad). Samples sizes were determined by performing small pilot studies or based on prior experience analyzing similar biological effects. Only one retina/eye was measured per animal, except in Fig. 2C where measurements in both eyes were taken. Damaged tissue was excluded from analysis, based on qualitative assessment. Differences between calculated averages were considered significant when $P<0.05$ using Student's t-test or one-way ANOVA tests. These tests were used because the data were normally distributed and no significant differences between variances were observed. All graphs presented in the Results section report mean±s.d., except in Fig. 6 where mean±s.e.m. is reported.

It is well characterized that, in normal murine retinas, S- and M-Opsin are expressed in an opposing dorsal-ventral gradient (Cepko, 1996; Roberts et al., 2006, 2007). To avoid any bias, for all cone quantifications (Fig. 5F and Fig. 8I), retinas were cryosectioned and all sections were immunostained and quantified; accordingly, the data are presented as number of cells per the whole retina.

To our knowledge, in contrast to other parts of the brain, gender differences in retinal patterning have not been observed. Young rodents (up to P30-60) do not show gender differences in vision (Chaychi et al., 2015), and the only minor sex-related differences in the retina observed to date are related to human color vision. These differences are mostly attributed to photopigment polymorphisms (Murray et al., 2012). Consequently, we did not separate our samples by gender. For western blot quantifications (Figs 3C, 8A and Fig. S3), we used films captured within the linear range to avoid saturation problems; next, the background was subtracted and densitometric values were obtained. All values were normalized using a β-actin blot obtained after stripping the same membrane or running the same samples with the same conditions in parallel. The number of experiments quantified per condition is indicated in the corresponding figure legend.

Acknowledgements

We thank Melissa Wong and Simranjeet Cheema for technical assistance; Dr Paul FitzGerald, Dr Nadean Brown, Dr Tom Glaser and Dr Jonathan Cooper for their generosity with both reagents and critical advice; Brad Shibata for assistance with tissue processing, and Dr Paul FitzGerald for invaluable help with EM and critical reading of the manuscript.

Competing interests

The authors declare no competing or financial interests.

Author contributions

Conceptualization: A.L.T., S.S.; Formal analysis: M.E.B., A.L.T., S.S.; Investigation: C.L.F., K.H., J.S.H., A.M.M., C.E.B., G.P.A.; Writing - original draft: A.L.T., S.S.; Writing - review & editing: A.L.T., S.S.; Visualization: A.L.T., S.S.; Supervision: A.L.T., S.S.; Funding acquisition: A.L.T., S.S.

Funding

This work was in part supported by the National Eye Institute (National Institutes of Health) [R01EY026942 to A.L.T.], by the National Institutes of Health T32 Vision Science Training grant [4T32EY015387-14] to C.L.F. (postdoctoral training grant) and to A.M.M. (graduate training grant). We also benefited from the use of the National Eye Institute Core Facilities [supported by P30 EY012576]. Deposited in PMC for release after 12 months.

Data availability

The data reported have been deposited in GEO under accession number GSE109465.

Supplementary information

Supplementary information available online at
http://dev.biologists.org/lookup/doi/10.1242/dev.155283.supplemental

References

Al-Awadi, S. A., Naguib, K. K., Farag, T. I., Teebi, A. S., Cuschieri, A., Al-Othman, S. A. and Sundareshan, T. S. (1986). Complex translocation involving chromosomes Y, 1, and 3 resulting in deletion of segment 3q23——q25. *J. Med. Genet.* **23**, 91-92.

Alvarado, M., Bocian, M. and Walker, A. P. (1987). Interstitial deletion of the long arm of chromosome 3: case report, review, and definition of a phenotype. *Am. J. Med. Genet.* **27**, 781-786.

Arnaud, L., Ballif, B. A. and Cooper, J. A. (2003a). Regulation of protein tyrosine kinase signaling by substrate degradation during brain development. *Mol. Cell. Biol.* **23**, 9293-9302.

Arnaud, L., Ballif, B. A., Förster, E. and Cooper, J. A. (2003b). Fyn tyrosine kinase is a critical regulator of disabled-1 during brain development. *Curr. Biol.* **13**, 9-17.

Baye, L. M. and Link, B. A. (2008). Nuclear migration during retinal development. *Brain Res.* **1192**, 29-36.

Beysen, D., Raes, J., Leroy, B. P., Lucassen, A., Yates, J. R., Clayton-Smith, J., Ilyina, H., Brooks, S. S., Christin-Maitre, S., Fellous, M. et al. (2005). Deletions involving long-range conserved nongenic sequences upstream and downstream of FOXL2 as a novel disease-causing mechanism in blepharophimosis syndrome. *Am. J. Hum. Genet.* **77**, 205-218.

Boyle, M. P., Bernard, A., Thompson, C. L., Ng, L., Boe, A., Mortrud, M., Hawrylycz, M. J., Jones, A. R., Hevner, R. F. and Lein, E. S. (2011). Cell-type-specific consequences of Reelin deficiency in the mouse neocortex, hippocampus, and amygdala. *J. Comp. Neurol.* **519**, 2061-2089.

Bringmann, A., Pannicke, T., Grosche, J., Francke, M., Wiedemann, P., Skatchkov, S. N., Osborne, N. N. and Reichenbach, A. (2006). Muller cells in the healthy and diseased retina. *Prog. Retin. Eye Res.* **25**, 397-424.

Carl, M. and Wittbrodt, J. (1999). Graded interference with FGF signalling reveals its dorsoventral asymmetry at the mid-hindbrain boundary. *Development* **126**, 5659-5667.

Cepko, C. L. (1996). The patterning and onset of opsin expression in vertebrate retinae. *Curr. Opin. Neurobiol.* **6**, 542-546.

Chang, B., Grau, T., Dangel, S., Hurd, R., Jurklies, B., Sener, E. C., Andreasson, S., Dollfus, H., Baumann, B., Bolz, S. et al. (2009). A homologous genetic basis of the murine cpfl1 mutant and human achromatopsia linked to mutations in the PDE6C gene. *Proc. Natl. Acad. Sci. USA* **106**, 19581-19586.

Chaychi, S., Polosa, A. and Lachapelle, P. (2015). Differences in retinal structure and function between aging male and female sprague-dawley rats are strongly influenced by the estrus cycle. *PLoS One* **10**, e0136056.

Chow, R. W., Almeida, A. D., Randlett, O., Norden, C. and Harris, W. A. (2015). Inhibitory neuron migration and IPL formation in the developing zebrafish retina. *Development* **142**, 2665-2677.

Close, J. L., Liu, J., Gumuscu, B. and Reh, T. A. (2006). Epidermal growth factor receptor expression regulates proliferation in the postnatal rat retina. *Glia* **54**, 94-104.

Dakubo, G. D., Wang, Y. P., Mazerolle, C., Campsall, K., McMahon, A. P. and Wallace, V. A. (2003). Retinal ganglion cell-derived sonic hedgehog signaling is required for optic disc and stalk neuroepithelial cell development. *Development* **130**, 2967-2980.

De Baere, E., Dixon, M. J., Small, K. W., Jabs, E. W., Leroy, B. P., Devriendt, K., Gillerot, Y., Mortier, G., Meire, F., Van Maldergem, L. et al. (2001). Spectrum of FOXL2 gene mutations in blepharophimosis-ptosis-epicanthus inversus (BPES) families demonstrates a genotype–phenotype correlation. *Hum. Mol. Genet.* **10**, 1591-1600.

Edqvist, P.-H. D. and Hallbook, F. (2004). Newborn horizontal cells migrate bi-directionally across the neuroepithelium during retinal development. *Development* **131**, 1343-1351.

Elshatory, Y., Everhart, D., Deng, M., Xie, X., Barlow, R. B. and Gan, L. (2007). Islet-1 controls the differentiation of retinal bipolar and cholinergic amacrine cells. *J. Neurosci.* **27**, 12707-12720.

Feng, L., Allen, N. S., Simo, S. and Cooper, J. A. (2007). Cullin 5 regulates Dab1 protein levels and neuron positioning during cortical development. *Genes Dev.* **21**, 2717-2730.

Franco, S. J., Martinez-Garay, I., Gil-Sanz, C., Harkins-Perry, S. R. and Müller, U. (2011). Reelin regulates cadherin function via Dab1/Rap1 to control neuronal migration and lamination in the neocortex. *Neuron* **69**, 482-497.
Furukawa, T., Kozak, C. A. and Cepko, C. L. (1997). rax, a novel paired-type homeobox gene, shows expression in the anterior neural fold and developing retina. *Proc. Natl. Acad. Sci. USA* **94**, 3088-3093.
Gao, Z. and Godbout, R. (2013). Reelin-disabled-1 signaling in neuronal migration: splicing takes the stage. *Cell. Mol. Life Sci.* **70**, 2319-2329.
Gao, Z., Monckton, E. A., Glubrecht, D. D., Logan, C. and Godbout, R. (2010). The early isoform of disabled-1 functions independently of Reelin-mediated tyrosine phosphorylation in chick retina. *Mol. Cell. Biol.* **30**, 4339-4353.
Goffinet, A. M. (1983). The embryonic development of the inferior olivary complex in normal and reeler (rlORL) mutant mice. *J. Comp. Neurol.* **219**, 10-24.
Hayashi, T., Cunningham, D., Bermingham-McDonogh, O. (2007). Loss of Fgfr3 leads to excess hair cell development in the mouse organ of Corti. *Dev. Dyn.* **236**, 525-533.
Hernández-Bejarano, M., Gestri, G., Spawls, L., Nieto-López, F., Picker, A., Tada, M., Brand, M., Bovolenta, P., Wilson, S. W. and Cavodeassi, F. (2015). Opposing Shh and Fgf signals initiate nasotemporal patterning of the zebrafish retina. *Development* **142**, 3933-3942.
Hoon, M., Okawa, H., Della Santina, L. and Wong, R. O. L. (2014). Functional architecture of the retina: development and disease. *Prog. Retin. Eye Res.* **42**, 44-84.
Howell, B. W., Hawkes, R., Soriano, P. and Cooper, J. A. (1997). Neuronal position in the developing brain is regulated by mouse disabled-1. *Nature* **389**, 733-737.
Icha, J., Kunath, C., Rocha-Martins, M. and Norden, C. (2016). Independent modes of ganglion cell translocation ensure correct lamination of the zebrafish retina. *J. Cell Biol.* **215**, 259-275.
Jimeno, D., Gomez, C., Calzada, N., de la Villa, P., Lillo, C. and Santos, E. (2016). RASGRF2 controls nuclear migration in postnatal retinal cone photoreceptors. *J. Cell Sci.* **129**, 729-742.
Katyal, S., Glubrecht, D. D., Li, L., Gao, Z. and Godbout, R. (2011). Disabled-1 alternative splicing in human fetal retina and neural tumors. *PLoS One* **6**, e28579.
Kolb, H., Linberg, K. A. and Fisher, S. K. (1992). Neurons of the human retina: a Golgi study. *J. Comp. Neurol.* **318**, 147-187.
Krol, A., Henle, S. J. and Goodrich, L. V. (2016). Fat3 and Ena/VASP proteins influence the emergence of asymmetric cell morphology in the developing retina. *Development* **143**, 2172-2182.
Lambert de Rouvroit, C. and Goffinet, A. M. (1998). The reeler mouse as a model of brain development. *Adv. Anat. Embryol. Cell Biol.* **150**, 1-106.
Lawrenson, I. D., Krebs, D. L., Linossi, E. M., Zhang, J. G., McLennan, T. J., Collin, C., McRae, H. M., Kolesnik, T. B., Koh, K., Britto, J. M. et al. (2017). Cortical layer inversion and deregulation of reelin signaling in the absence of SOCS6 and SOCS7. *Cereb. Cortex* **27**, 576-588.
Malicki, J., Jo, H. and Pujic, Z. (2003). Zebrafish N-cadherin, encoded by the glass onion locus, plays an essential role in retinal patterning. *Dev. Biol.* **259**, 95-108.
Marc, R. E., Anderson, J. R., Jones, B. W., Sigulinsky, C. L. and Lauritzen, J. S. (2014). The AII amacrine cell connectome: a dense network hub. *Front. Neural. Circuits* **8**, 104.
Martsolf, J. T. and Ray, M. (1983). Interstitial deletion of the long arm of chromosome 3. *Ann. Genet.* **26**, 98-99.
Matsunaga, M., Hatta, K. and Takeichi, M. (1988). Role of N-cadherin cell adhesion molecules in the histogenesis of neural retina. *Neuron* **1**, 289-295.
Maurer, K. A., Riesenberg, A. N. and Brown, N. L. (2014). Notch signaling differentially regulates Atoh7 and Neurog2 in the distal mouse retina. *Development* **141**, 3243-3254.
Miyata, T. and Ogawa, M. (2007). Twisting of neocortical progenitor cells underlies a spring-like mechanism for daughter-cell migration. *Curr. Biol.* **17**, 146-151.
Miyata, T., Nakajima, K., Mikoshiba, K. and Ogawa, M. (1997). Regulation of Purkinje cell alignment by reelin as revealed with CR-50 antibody. *J. Neurosci.* **17**, 3599-3609.
Morgan, J. and Wong, R. (1995). Development of cell types and synaptic connections in the retina. In *Webvision: The Organization of the Retina and Visual System* (ed. H. Kolb, E. Fernandez and R. Nelson). Salt Lake City, UT: University of Utah School of Medicine. webvision.med.utah.edu/
Morgan, J. L., Dhingra, A., Vardi, N. and Wong, R. O. L. (2006). Axons and dendrites originate from neuroepithelial-like processes of retinal bipolar cells. *Nat. Neurosci.* **9**, 85-92.
Murray, I. J., Parry, N. R., McKeefry, D. J. and Panorgias, A. (2012). Sex-related differences in peripheral human color vision: a color matching study. *J. Vis.* **12**, 18.
Nadarajah, B., Brunstrom, J. E., Grutzendler, J., Wong, R. O. L. and Pearlman, A. L. (2001). Two modes of radial migration in early development of the cerebral cortex. *Nat. Neurosci.* **4**, 143-150.
Nelson, B. R., Hartman, B. H., Georgi, S. A., Lan, M. S. and Reh, T. A. (2007). Transient inactivation of Notch signaling synchronizes differentiation of neural progenitor cells. *Dev. Biol.* **304**, 479-498.
Nguyen-Ba-Charvet, K. T. and Chédotal, A. (2014). Development of retinal layers. *C. R. Biol.* **337**, 153-159.
Okumura, F., Joo-Okumura, A., Nakatsukasa, K. and Kamura, T. (2016). The role of cullin 5-containing ubiquitin ligases. *Cell Div.* **11**, 1.
Peinado Allina, G., Fortenbach, C., Naarendorp, F., Gross, O. P., Pugh, E. N., Jr. Burns, M. E. (2017). Bright flash response recovery of mammalian rods in vivo is rate limited by RGS9. *J. Gen. Physiol.* **149**, 443-454.
Petroski, M. D. and Deshaies, R. J. (2005). Function and regulation of cullin-RING ubiquitin ligases. *Nat. Rev. Mol. Cell Biol.* **6**, 9-20.
Poggi, L., Vitorino, M., Masai, I. and Harris, W. A. (2005). Influences on neural lineage and mode of division in the zebrafish retina in vivo. *J. Cell Biol.* **171**, 991-999.
Prasov, L. and Glaser, T. (2012). Pushing the envelope of retinal ganglion cell genesis: context dependent function of Math5 (Atoh7). *Dev. Biol.* **368**, 214-230.
Razafsky, D., Blecher, N., Markov, A., Stewart-Hutchinson, P. J. and Hodzic, D. (2012). LINC complexes mediate the positioning of cone photoreceptor nuclei in mouse retina. *PLoS One* **7**, e47180.
Rea, G., McCullough, S., McNerlan, S., Craig, B. and Morrison, P. J. (2010). Delineation of a recognisable phenotype of interstitial deletion 3 (q22.3q25.1) in a case with previously unreported truncus arteriosus. *Eur. J. Med. Genet.* **53**, 162-167.
Rice, D. S. and Curran, T. (2000). Disabled-1 is expressed in type AII amacrine cells in the mouse retina. *J. Comp. Neurol.* **424**, 327-338.
Rice, D. S. and Curran, T. (2001). Role of the reelin signaling pathway in central nervous system development. *Annu. Rev. Neurosci.* **24**, 1005-1039.
Rice, D. S., Nusinowitz, S., Azimi, A. M., Martinez, A., Soriano, E. and Curran, T. (2001). The reelin pathway modulates the structure and function of retinal synaptic circuitry. *Neuron* **31**, 929-941.
Rich, K. A., Zhan, Y. and Blanks, J. C. (1997). Migration and synaptogenesis of cone photoreceptors in the developing mouse retina. *J. Comp. Neurol.* **388**, 47-63.
Roberts, M. R., Srinivas, M., Forrest, D., Morreale de Escobar, G. and Reh, T. A. (2006). Making the gradient: thyroid hormone regulates cone opsin expression in the developing mouse retina. *Proc. Natl. Acad. Sci. USA* **103**, 6218-6223.
Roberts, S., Gordon, A., McLean, C., Pedersen, J., Bowden, S., Thomson, K. and Angus, P. (2007). Effect of sustained viral response on hepatic venous pressure gradient in hepatitis C-related cirrhosis. *Clin. Gastroenterol. Hepatol.* **5**, 932-937.
Robles, E. and Baier, H. (2012). Assembly of synaptic laminae by axon guidance molecules. *Curr. Opin. Neurobiol.* **22**, 799-804.
Rodieck, R. W. (1973). *The Vertebrate Retina; Principles of Structure and Function*. San Francisco: Freeman.
Schmitz, F. (2009). The making of synaptic ribbons: how they are built and what they do. *Neuroscientist* **15**, 611-624.
Shen, W., Fruttiger, M., Zhu, L., Chung, S. H., Barnett, N. L., Kirk, J. K., Lee, S., Coorey, N. J., Killingsworth, M., Sherman, L. S. et al. (2012). Conditional Mullercell ablation causes independent neuronal and vascular pathologies in a novel transgenic model. *J. Neurosci.* **32**, 15715-15727.
Shen, N., Qu, Y., Yu, Y., So, K.-F., Goffinet, A. M., Vardi, N., Xu, Y. and Zhou, L. (2016). Frizzled3 shapes the development of retinal rod bipolar cells. *Invest. Ophthalmol. Vis. Sci.* **57**, 2788-2796.
Simó, S. and Cooper, J. A. (2013). Rbx2 regulates neuronal migration through different cullin 5-RING ligase adaptors. *Dev. Cell* **27**, 399-411.
Simo, S., Jossin, Y. and Cooper, J. A. (2010). Cullin 5 regulates cortical layering by modulating the speed and duration of Dab1-dependent neuronal migration. *J. Neurosci.* **30**, 5668-5676.
Sun, N., Shibata, B., Hess, J. F. and FitzGerald, P. G. (2015). An alternative means of retaining ocular structure and improving immunoreactivity for light microscopy studies. *Mol. Vis.* **21**, 428-442.
Tallquist, M. D. and Soriano, P. (2000). Epiblast-restricted Cre expression in MORE mice: a tool to distinguish embryonic vs. extra-embryonic gene function. *Genesis* **26**, 113-115.
Tissir, F. and Goffinet, A. M. (2003). Reelin and brain development. *Nat. Rev. Neurosci.* **4**, 496-505.
Trifunović, D., Dengler, K., Michalakis, S., Zrenner, E., Wissinger, B. and Paquet-Durand, F. (2010). cGMP-dependent cone photoreceptor degeneration in the cpfl1 mouse retina. *J. Comp. Neurol.* **518**, 3604-3617.
Trommsdorff, M., Gotthardt, M., Hiesberger, T., Shelton, J., Stockinger, W., Nimpf, J., Hammer, R. E., Richardson, J. A. and Herz, J. (1999). Reeler/Disabled-like disruption of neuronal migration in knockout mice lacking the VLDL receptor and ApoE receptor 2. *Cell* **97**, 689-701.
Trotter, J. H., Klein, M., Jinwal, U. K., Abisambra, J. F., Dickey, C. A., Tharkur, J., Masiulis, I., Ding, J., Locke, K. G., Rickman, C. B. et al. (2011). ApoER2 function in the establishment and maintenance of retinal synaptic connectivity. *J. Neurosci.* **31**, 14413-14423.
Ueki, Y. and Reh, T. A. (2013). EGF stimulates Muller glial proliferation via a BMP-dependent mechanism. *Glia* **61**, 778-789.
Ueki, Y., Wilken, M. S., Cox, K. E., Chipman, L. B., Bermingham-McDonogh, O. and Reh, T. A. (2015). A transient wave of BMP signaling in the retina is necessary for Muller glial differentiation. *Development* **142**, 533-543.
Zahanova, S., Meaney, B., Labieniec, B., Verdin, H., De Baere, E. and Nowaczyk, M. J. (2012). Blepharophimosis-ptosis-epicanthus inversus syndrome plus: deletion 3q22.3q23 in a patient with characteristic facial features and with genital anomalies, spastic diplegia, and speech delay. *Clin. Dysmorphol.* **21**, 48-52.